MASTER THESIS

Augmented reality in cranio-maxillofacial surgery

Thijs Bussink, BSc.

Technical Medicine, University of Twente

3D Lab, Radboud UMC Nijmegen

Department of Craniomaxillofacial Surgery, Radboud UMC Nijmegen

29 January 2020

EXAMINATION COMMITTEE

Dr. Ir. F. van der Heijden	(Chairman & Technical Supervisor)
Dr. W.A. Borstlap	(Medical Supervisor)
Drs. A.G. Lovink	(Process Supervisor)
Drs. J.W. Meulstee	(External Member)

3DLab Radboudumc

UNIVERSITY OF TWENTE.

Preface

In de 4e klas van de middelbare school kwam ik er eigenlijk al achter dat ik Technische Geneeskunde wilde gaan studeren. Ik had altijd al wel interesse in geneeskunde, maar ik was ook erg technische aangelegd en bèta vakken waren mijn favoriet. Tijdens een studiekeuze markt ben ik bij een presentatie over Technische Geneeskunde beland en toen wist ik het, dit is wat ik wil gaan studeren. En zo geschiedde het, ik ging een kleine 3 jaar later naar Enschede toe om Technische Geneeskunde te gaan studeren.

Na de bachelor in 3 jaar te hebben afgerond, ben ik aan de master track Medical Imaging & Interventions begonnen. Om mijn studententijd niet te snel voorbij te laten gaan heb ik mij tijdens mijn master ook nog bezig gehouden met het organiseren van een studiereis naar China. Maar daarna werd het tijd om stage te gaan lopen en mij verder te gaan ontwikkelen. Na twee leerzame stages in het Antoni van Leeuwenhoek en het VUmc kwam ik voor het eerst op het 3D lab in het RadboudUMC terecht. Deze stage heb ik Jene Meulstee ook leren kennen als stagebegeleider. Tijdens de stage kwam ik voor het eerst in aanraking met Augmented Reality(AR) en heb ik onderzoek gedaan naar het visualiseren van patiënt specifieke anatomie op de patiënt, met als doel dit toe te gaan passen voor de DIEP-lap borstreconstructies bij de plastische chirurgie. AR heeft tijdens deze stage zoveel interesse opgewekt, dat ik besloot dat ik daar ook mijn thesis over wilde gaan schrijven.

Na mijn laatste korte stage in Tilburg heb ik weer contact opgenomen met Jene Meulstee om te kijken op welk HoloLens project ik zou kunnen gaan afstuderen, dat heeft uiteindelijk geleidt tot het onderzoek wat nu voor u ligt. Jene Meulstee heeft zelf veel onderzoek gedaan naar craniosynostose en het gebruik van virtuele planningen bij craniosynostose, alleen de mogelijkheid om daarbij AR te gaan gebruiken kon nog uitgebreider onderzocht worden. Daarom hebben we als doel voor mijn afstuderen gesteld om te onderzoeken wat de mogelijkheden zijn om deze virtuele planningen over te brengen met AR, hoe nauwkeurig dit kan in vergelijking met chirurgische malletjes en of dit ook toepasbaar zou zijn voor andere operaties.

Tijdens het afstuderen kon ik mijn technische kennis en vaardigheden verder ontwikkelen, doordat ik weer verder kon met het programmeren voor de HoloLens, maar ook mocht helpen bij het plannen van de open reconstructies van craniosynostose. Het ontwikkelproces was veel trial-and-error, maar heeft uiteindelijk wel geleidt tot een applicatie, die zonder gebruik van andere technieken, alle aspecten van de virtuele planningen kon visualiseren en nauwkeurig kon overbrengen op de patiënt. Deze applicatie is in oktober 2019 ook in het tv-programma TopDoks te zien geweest. Om te bepalen hoe nauwkeurig de ontwikkelde applicatie was hebben we een fantoomstudie uitgevoerd, waarbij we gekeken hebben hoe nauwkeurig de HoloLens was in vergelijking chirurgische mallen, de gouden

standaard. Helaas is het niet gelukt om de nauwkeurigheid van de mallen te behalen met de applicatie, desondanks waren de resultaten wel veel belovend en zijn dan ook samengevat in een artikel wat opgestuurd is voor publicatie.

Binnen de afdeling MKA is in het afgelopen jaar ook steeds meer interesse gekomen voor het toepassen van AR. Kort nadat we het onderzoek hadden uitgevoerd zijn we benaderd door Tong Xi met de vraag of we AR niet konden gebruiken voor een proportionele condylectomy. Met een paar kleine aanpassingen in de gemaakte applicatie en met behulp van de steriele QR codes die door Gijs Luijten zijn gemaakt, hebben we dit ook snel kunnen uitvoeren. Ook hieruit is een kort artikel gekomen welke opgestuurde is voor publicatie.

Op klinisch gebied heb ik mij veel kunnen ontwikkelen tijdens het afgelopen jaar, zo heb ik regelmatig het craniosynostose spreekuur over kunnen nemen. Tijdens dit spreekuur liet ik aan de ouders van patiënten uitgebreide analyses zien van de 3D foto's de gemaakt zijn, om zo te kunnen laten zien wat het effect is geweest van de operatie en de daaropvolgende helm therapie. Deze spreekuren zijn ook precies wat ik mij altijd heb voorgesteld bij Technische Geneeskunde, technische en medische kennis combineren om een bijdrage te leveren aan de zorg.

Ik hoop alles wat ik geleerd heb afgelopen jaren samen te kunnen brengen in de nieuwe uitdagingen die ik aanga na het behalen van mijn master diploma. Te beginnen met een promotie onderzoek op de plastische chirurgie, waar voor mij het avontuur van AR begonnen is.

Ik wil graag Jene Meulstee bedanken voor de begeleiding het afgelopen jaar, de mooie projecten die we samen op hebben kunnen pakken en alle feedback die ik heb mogen ontvangen. Ook wil ik Wilfred Borstlap bedanken voor de medische begeleiding, de feedback op mijn geschreven stukken en de input voor het onderzoek. Daarnaast wil ik ook Ferdinand van der Heijden bedanken voor de spar momenten die we gehad hebben en de technische begeleiding en Annelies Lovink voor de procesbegeleiding en de daarbij behorende goede gesprekken. Tot slot wil ik ook mijn ouders bedanken voor de interesse die ze altijd gehad hebben in mijn studie en voor het steunen van de keuzes die hebben geleidt tot waar ik nu ben.

Ik wens u veel leesplezier toe.

Thijs Bussink

Nijmegen, 29 januari 2019

Abstract

Introduction

Craniosynostosis is a congenital disorder that leads to an abnormal cranial shape and possibly increased intracranial pressure. Open cranial vault reconstruction(OCVR) is an surgical method for the treatment of craniosynostosis. The goal of this intervention is to increase the intracranial volume and create a more natural cranial shape. Virtual surgical planning(VSP) provides the possibility to simulate different strategies for the open cranial reconstruction prior to surgery. Although surgical guides can be used to transfer the virtual surgical plan to the patient during surgery, producing these guides is time consuming and rather expensive. Augmented reality(AR) is a 3D visualization technique that can be used to visualize and transfer the virtual planning onto the patient in the operation room in an intuitive, accurate and low-cost way.

Materials & Methods

To realize the transfer of the VSP, an application for the Microsoft HoloLens, a pair of AR glasses, was developed. Using quick response(QR) codes and a tracking algorithm, point-based registration and real-time tracking were implemented. To accurately transfer the osteotomy pattern, a navigational transfer method was implemented. The created workflow was compared to the conventional method of surgical guides by using 3D prints of 10 patients suffering from different types of craniosynostosis. Each method was tested by two observers at two different moments. To analyze the delineations of the osteotomy patterns on the 3D prints, an improved trilateration method was developed and validated.

Results

The created application allowed accurate visualization of the osteotomy pattern and reconstruction phase of the VSP. The improved trilateration method showed to be an accurate method for analyzing the delineations. Surgical guides were the most accurate method to transfer the planning to the patient with a mean accuracy of 0.9 ± 0.6 mm and a mean transfer time of 50 seconds. The AR workflow resulted in an accuracy of 2.1 ± 1.5 mm, with outliers up to 8 mm, and a transfer time of 8 minutes and 24 seconds on average. Transfer time and accuracy were significant different between observers.

Conclusion

Even though the results showed that the AR transfer method is not as accurate as the surgical guides and required a longer transfer time, this method is promising and hopefully clinically applicable for OCVR with the proper training and prevention of outliers. And with the proposed improvements and the introduction of the Hololens 2, AR has the potential to revolutionize the way VSP's are used and created.

Contents

List of figures

List of tables

List of abbreviations

2D	Two Dimensional
3D	Three Dimensional
ANOVA	Analysis of Variance
AR	Augmented Reality
CBCT	Cone Beam Computed Tomography
CMF	CranioMaxilloFacial
CT	Computed Tomography
EASC	Endoscopic Assisted Strip Craniectomy
EM	ElectroMagnetic
HMD	Head Mounted Display
FOV	Field Of View
ICC	Intraclass Correlation Coefficient
ICP	Intra Cranial Pressure
OCVR	Open Cranial Vault Reconstruction
ONS	Optical Navigation System
OR	Operating Room
OST-HMD	Optical See-Through Head Mounted Display
PET	Positron Emisson Tomography
QR	Quick Response
RMS(E)	Root-Mean Squared (Error)
SDK	Software Development Kit
SVD	Singular Value Decomposition
UCH	Unilateral Condylar Hyperplasia
VSP	Virtual Surgery Planning

Part 1

Transfer of virtual surgical planning for open cranial vault reconstruction

1. Introduction

1.1 Craniosynostosis

The developing human skull can be divided into two parts, the neurocranium and the viscerocranium. The first forms the part of the skull that protects the brain and the latter the part that forms the facial bones. The neurocranium can be divided into a membranous part, the flat bones, which surround the brain, and the cartilaginous part, which forms the bones of the base of the skull. The flat bones in a new born are separated by narrow seams of connective tissue, called sutures. These sutures have derived from two different sources, neural crest cells and the paraxial mesoderm, the sagittal suture and coronal sutures respectively. At the places where more than two flat bones connect, the sutures are wider and form a fontanelle. This connective tissue between the bones of the skull allows them to overlap during birth and move back to their original position soon after birth. The sutures and fontanelles remain membranous for a considerable amount of time.[1] The metopic suture is usually the first one to close at two years of age. All other sutures close in adulthood after completion of craniofacial growth, allowing the infant's brain to grow rapidly. Within the first two years after birth, the infant's brain grows to about 75% of its adult volume, with the remaining 25% of growth taking place in the years until adulthood.[2]

Premature closure of one or more of these sutures is called craniosynostosis and the first cases were described in 1851.[3] Craniosynostosis occurs in 1 of every 1500-1600 births in the Netherlands, which results in 110 new cases each year.[4] This condition can be divided into different subtypes depending on which sutures have closed prematurely, see Figure 1. Scaphocephaly, premature closure of the sagittal suture, is the most prevalent form of craniosynostosis (42-46%), followed by trigonocephaly (26-33%), premature closure of the metopic suture.[4–7] The third form of single suture craniosynostosis is plagiocephaly which is caused by premature closure of one of the coronal or lambdoid sutures.[7] Besides these type of single suture craniosynostosis, there are also several types which include more than one suture; brachycephaly, oxycephaly, triphyllocephaly.[4] Craniosynostosis can also be divided into a non-syndromic and a syndromic category, Over 150 different syndromes have been associated with craniosynostosis[6] and they account for about 8% of all the cases of craniosynostosis. Apert, Crouzon and Pfeiffer syndromes are a few examples of syndromes associated with craniosynostosis and in most of these syndromes the fibroblast growth factor receptor gene is involved. [8]

Craniosynostosis is associated with restriction of the brain development and can lead to increased intracranial pressure(ICP)[9], impairments of cognitive and neurodevelopment function[10–12], deficits in speech[13], hearing and vision and will also have aesthetic consequences due to an abnormal skull shape.[14]

The incidence of these symptoms increase when more than one suture is involved.[15] Multi-suture craniosynostosis, can also lead to Chiari malformations[16], a displacement of the cerebellum, alone or with the lower medulla oblongata, into the spinal canal.[17]

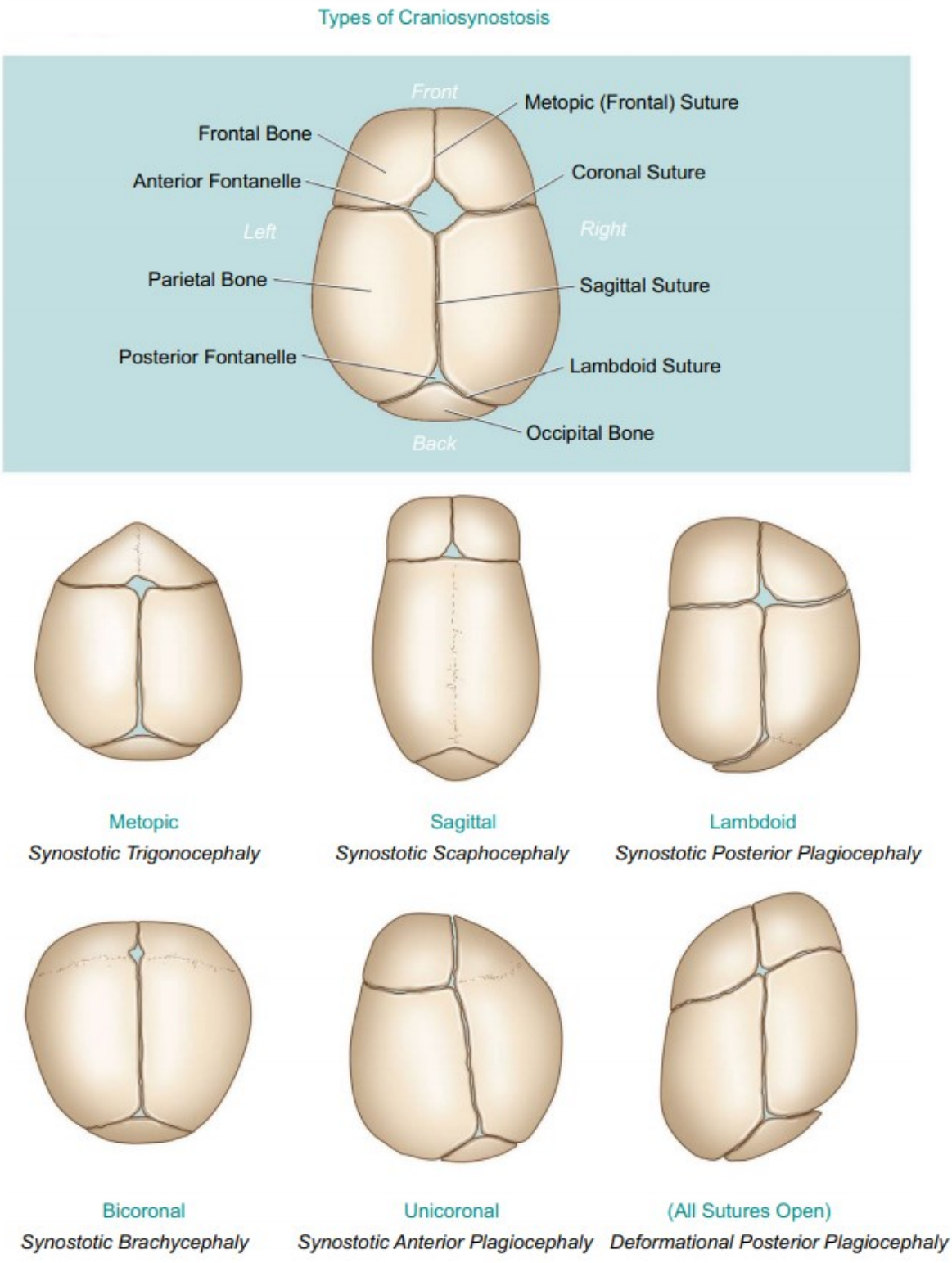

Figure 1 Normal cranial anatomy (top) and 6 types of craniosynostosis (bottom). [93]

1.2 Treatment

To decrease the risk of increased ICP and the resulting symptoms, surgical management is the current best practice, both for syndromic and non-syndromic craniosynostosis.[18,19] The first surgical procedure was described by Lannelongue in 1890, starting with release of the closed suture.[20] Since then, techniques have rapidly developed, focusing on early intervention and less invasive procedures.[21] In the RadboudUMC, the first choice of surgical intervention for non-syndromic craniosynostosis is endoscopic assisted strip craniectomy (EASC).[22] A technique that was initially presented by Jimenez and Barone[23,24] and introduced in the RadboudUMC in 2005. Using an endoscope, a traditional strip craniectomy can be performed via a small incision perpendicular to the closed suture. The goal of the surgery is to remove the suture, to allow the infant's skull to continue to grown along the resected suture.[25] Postoperatively helmet therapy is indicated after EASC, the helmet is worn for several month and is specially designed to allow the skull to grow more in the direction its growth was restricted in before surgery.[26] The helmets can be worn up to 12 months after surgery to direct the growth.[27] In our center, helmet therapy is continued, on average, for 10 months postoperative.[22]

Despite all studies on EASC and their promising results, open cranial vault reconstruction (OCVR) is still the most commonly used method to treat craniosynostosis.[18,28,29] Studies comparing EASC with OCVR have shown that EASC results in fewer transfusions, less operation and post-operative hospital time, less complications and overall costs. [22,30–34] Outcomes of EASC are best when surgery is performed as early as possible, preferably within 3 months after birth but no more than 6 months.[8,33,35] Therefore, OCVR is indicated in our institution, in case patients have not had surgery within this time window or in case of severe cranial deformities.[22,36] OCVR starts with a coronal incision, to create access to the patient's cranium. Next, depending on the type of craniosynostosis, part of the cranium is resected and reconstructed to increase the cranial volume and correct the shape. In case of scaphocephaly, part of the cranial vault including the closed sagittal suture is resected. Thereafter, the cranial vault is remodeled such that the intracranial volume is increased. In case of trigonocephaly, part of the cranial vault including the closed metopic suture and the orbital bandeau is resected. The orbital bandeau is reshaped to increase the angle between the orbita in the axial plane. The parts of the cranial vault are reconstructed after the orbital bandeau to increase the intracranial volume and create a more natural appearing forehead. In case of plagiocephaly, the procedure is similar to the procedure for trigonocephaly. But instead of reconstructing the entire forehead, only the side with the closed coronal suture is reconstructed to match the contralateral side and create a more symmetrical forehead with an increased intracranial volume.[7,37]

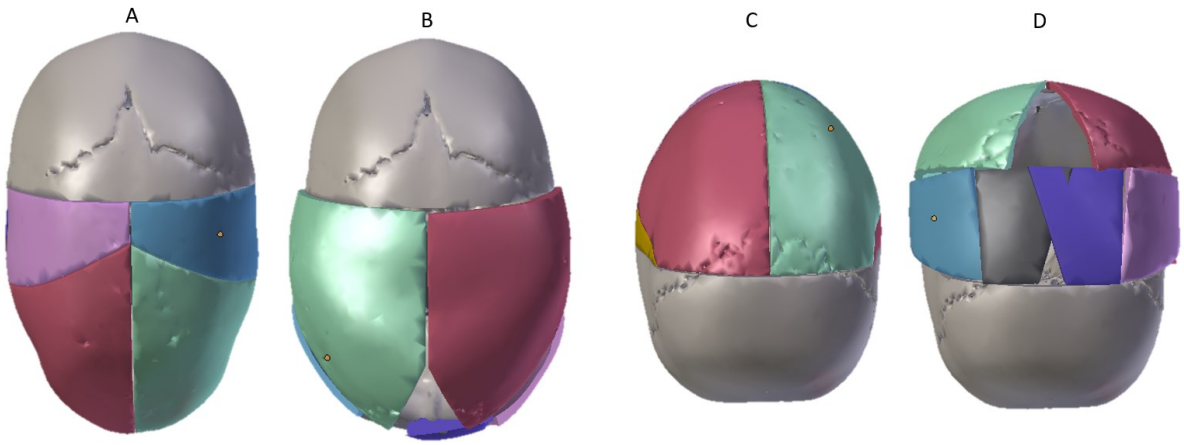

Figure 2 Example of a VSP for scaphocephaly, wherein the osteotomy pattern and resulting cranial segments are shown (A and C) and how these segments should be placed in the reconstruction phase to achieve the desired result (B and D).

1.3 Virtual surgical planning

With the advancements in three-dimensional (3D) modeling techniques, a virtual surgical planning (VSP) of the OCVR can be created. From the computed tomography (CT) scan that is made preoperatively, a 3D model of the skull of the patient can be created on which the resection of the cranial segments and their reconstruction can be virtually simulated. This allows the surgeons to explore several options for the osteotomy and the reconstruction of the segments before performing the surgery.[38–41] VSP decreases the time needed for surgery[42] and enables the surgeon to gain a greater understanding of the patient's anatomy.[43] In the RadboudUMC, this VSP consist of two parts, one part describing the osteotomy pattern and one part visualizing how the resected cranial segments have to be reconstructed, see Figure 2. This osteotomy pattern is drawn on the patient's cranium intraoperative using a caliper, a surgical marker and anatomical landmarks. Transferring the VSP is a time-consuming process, prone to errors and dependent on visible anatomical landmarks which are not always available. Another method for transfer of the VSP is the use of 3D printed patient specific cutting guides and reconstruction templates, allowing for a faster transfer, reduced operation time and intraoperative blood loss.[38,41,44–52] The combination of preoperative planning and intraoperative guides also generates quantitative surgical goals and allows for an accurate reproduction of the planned results.[43] However, designing these guides is a time consuming process costing 1-2 days. Production of these guides costs up to €2000 and up to €6000 including overhead costs which mostly consist of the labor costs to design the guides.[45,50,53] In 2019 the first OCVR using surgical guides was performed in our institution. A guide was made to transfer the osteotomy pattern onto the patient, and several smaller guides where made to help the surgeon put the cranial segments back together. The use of these guides decreased the time needed to transfer the VSP onto the patient, but were expensive to manufacture and sterilize.

Therefore, Augmented Reality (AR) is explored to overcome these cost issues and utilize the VSP to its full extend, which will be further explained in the following section.

1.4 Augmented reality

1.4.1 History of AR

AR, also known as mixed-reality, is a concept where advanced visualization techniques are used to enhance the real world with virtual object. Despite rapid development of the technology in the second half of the 20th century, utilization of AR in medicine did not start until the end of the 20th century. Some people argue that 'The Character Marker' in the novel 'The Master Key' by L. Frank Baum was the first time the concept of AR was mentioned. Described as 'A pair of spectacles, while you wear them everyone you meet will be marked upon the forehead with a letter indicating his or her character'.[54] A pair of spectacles which sound a lot like the immersive headsets we use nowadays. Earlier implementations of AR added two-dimensional (2D) projections onto 2D images. Nowadays, AR is a system that is able to combine the real and virtual worlds with real-time interactions and an accurate 3D registration of both virtual and real objects.[55]

In 1995, Wagner et al. were one of the first to use the term and concept of AR in the field of medicine. They presented a visualization system for imaged guided surgery, with a semi-immersive head-mounted display (HMD) and camera. However, most advances of AR in medicine have been made in the previous decade, even though the term and concept have been around for more than two decades. A PubMed search shows that the amount of publications a year on AR increased sixfold over the past decade, with over a third on the combination of AR and surgery, see Figure 3.

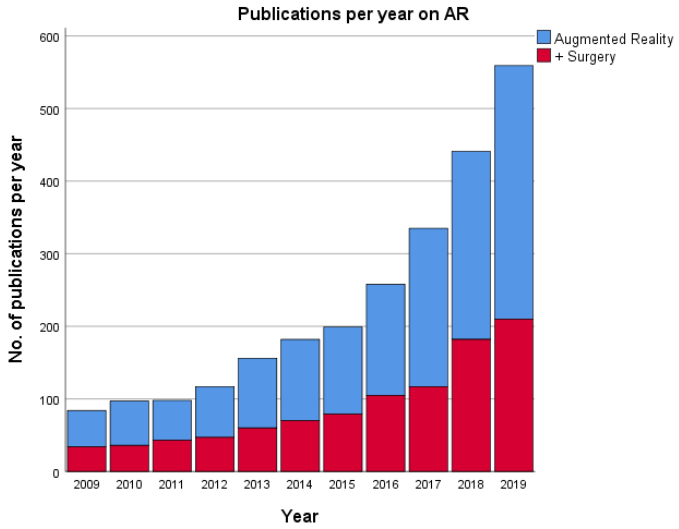

Figure 3 Number of publications on AR and AR combined with surgery per year.

1.4.2 AR glasses

The latest development in the field of AR has been the introduction of commercially available head-mounted AR-glasses. One of the first was the Google Glass, introduced in 2013, and resembling a normal pair of glasses, equipped with a small screen and a camera. Doctors were among the early adopters of these glasses[56], using them to easily record[57] and live stream[58] surgery for educational purposes, to visualize vital signs[59,60] during surgery or to display neuronavigational data directly in the surgeons field of view[61]. However, the Google Glass only allowed 2D perception of the displayed information and was not able to track its environment. Making it less suitable for visualisation of a 3D VSP. Therefore, a more immersive type of AR glasses are needed, the so called optical see-through head-mounted displays(OST-HMD). Equipped with two see-through displays to allow 3D visualization and several sensors and cameras to track its surrounding, allowing for a fluent integration of the real and virtual world. This enables the use of the VSP in 3D, which is otherwise only observed on a screen in 2D.

Qian et al. presented one of the first papers on OST-HMD in 2017, with an approach to evaluate OST-HMD for specific clinical situations. Their approach showed that the Microsoft HoloLens, introduced in 2016, was the most suitable as 'object-anchored 2D-display' during interventions, compared to the Epson Moverio BT-200 and the ODG R-7.[62] Moosburner et al. published a similar article last year, comparing the HoloLens to the Meta 2. They concluded that, despite its limited field of view, the HoloLens had some key advantages which could be beneficial in a surgical setting.[63] This suggest that the HoloLens (Figure 4) is the currently best OST-HMD that is commercially available and with a price of a €3000 it is a suitable candidate for transferring a VSP onto a patient.

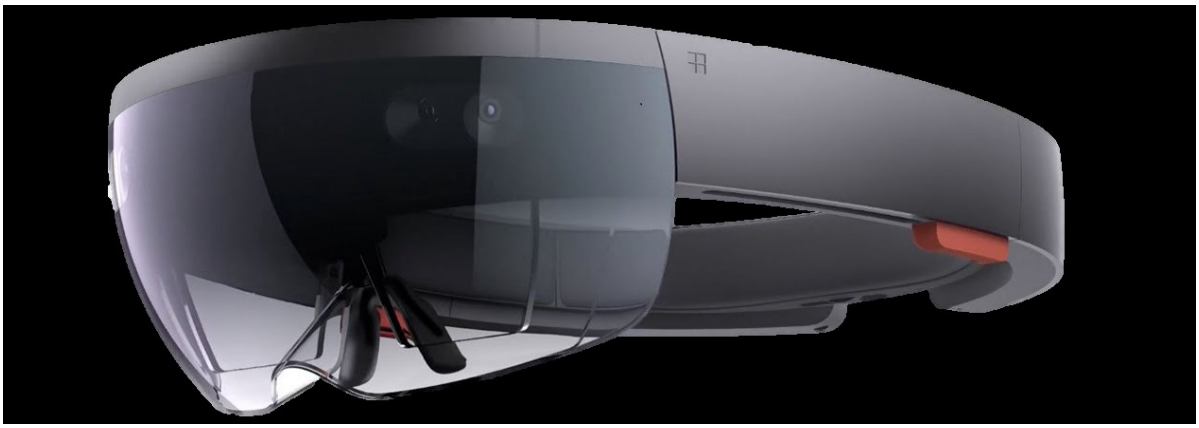

Figure 4 The Microsoft HoloLens.

1.4.3 HoloLens implementations

In 2018, Pratt et al. published one of the first papers on perioperative use of the HoloLens. They created an application to visualize perforating vessels in the extremities during reconstructive surgery. Using voice-commands and hand-gestures, the surgeon was able to place the models of the extremity over the patient.[64] Incekara et al. published a similar article on the visualization and transfer of the outline of brain tumors on the patient's skin, using manual surface registration.[65] Li et al. did the same for the placement of extra ventricular drains, using virtual markers that corresponded with physical markers to determine if their registration was correct.[66] These studies are promising, but there is one major disadvantage of the used method. Manual alignment means the patient is not actively tracked during the procedure, requiring the surgeon to correct the placement of the models after manipulation of the patient. Besides this, manual alignment is also prone to human induced errors and the accuracy is highly dependent on the user's experience with the HoloLens.

Real-time tracking of the patient can eliminate these errors and enable an accurate registration of the patient. An optical navigation system (ONS) using infrared cameras is one of the techniques that has been described in combination with the HoloLens to allow real-time tracking and increase the accuracy of the HoloLens. Kuzhagaliyev et al. presented such a system, developed for irreversible electroporation of pancreas tumors, to track the progress of the needle insertion and to visualize the target needle trajectory.[67] Meulstee et al. presented a similar system, not for a specific intervention, but to asses the influence of the HoloLens on the accuracy on the ONS.[68] Combining AR with an ONS sounds promising, especially since these systems have already proven their accuracy and added value in, among others, the field of neuro- and craniomaxillofacial(CMF) surgery.[69,70] However, these systems are expensive compared to the HoloLens, always have to have the surgical field in line of sight and are not available in every operating room (OR).

Electromagnetic (EM) tracking is another technique that has been described in combination with the HoloLens to implement real-time tracking. Kuhlemann et al. presented such a system for endovascular interventions, where they linked an EM tracking system to the HoloLens to visualize an EM catheter inside the patient.[71] Their system is promising in the search for reducing radiation exposure during endovascular repairs. However, it still requires an additional device to be brought into the OR and this device is not readily available at the 3D Lab.

Utilization of image tracking is yet another technique that has been described to track the patient's position in real-time, using the integrated camera of the HoloLens. Image tracking is based on the

feature detection in contrast rich images(image targets), from which a computer can determine its position and orientation. Several implementations have been described in literature. Moreta-Martinez et al. created a patient specific guide for the patient's tibia, with an image target attached to it. They created an application that positioned the holograms based on the position of the image target.[72] The proposed technique allowed real-time tracking of the patient and had a high accuracy, however this technique is still prone to errors due to misplacement of the guide. Müller et al. used a similar technique for the placement of spinal pedicle screws. Patient specific guides were used to track a cadaver and a pointer with an image target attached to it was used to position the screws.[73] This form of tracking the patient is promising, but it still requires expensive patient specific guides.

Different implementations of image tracking have been described as well, Van Doormaal et. al used image tracking for point-based registration of the patient. A pointer with a quick response (QR) code attached to it was used to mark fiducials placed on the patient's head. Since the patient's head was fixated, only one registration was needed.[74] One flaw in their design was that it solely depends on how the HoloLens tracks its environment, as the HoloLens is prone to errors caused by drifting of the virtual objects.[75]

1.4.4 Accuracy

An accurate and detailed preoperative plan demands an accurate transfer method. If a VSP cannot be performed correctly during surgery, it may lead to a suboptimal result. Therefore, an accurate method for tracking and registration of the patient has to be chosen. Using manual alignment, accuracies of 4 mm[65,66] have been described, comparable to those of EM tracking combined with AR.[71] Meulstee et al. were able to reach an accuracy of 2.3 mm when combining ONS with AR.[68] The use of image targets resulted in an accuracy of 2.9 mm when used for real-time tracking on patient specific guides[72] and 4.4 mm when used for point based registration.[76]

In case of OCVR, an error margin of 2 mm is deemed acceptable when a VSP is transferred onto the patient. This is due to the fact that transfer of the planning with a surgical marker, handling of the craniotome and the thickness of the osteotomy will always induce a small error. Therefore, an error margin lower than 2 mm will have limited effect on the final result. Using an ONS seems to be the best candidate to achieve this. However, using an ONS in combination with the HoloLens will be as expensive as surgical guides and requires additional devices to be brought into the OR. The second most accurate technique, is real-time tracking of image targets placed on patient specific guides. Han et al. have presented such a method for plagiocephaly reconstructions, using occlusal splints.[77] However, this still

requires expensive patient specific splints with an trackable image attached to it and in case of scaphocephaly, patients are place in sphinx position making the mouth inaccessible for placement of the occlusal splint. To overcome these issues, the most suitable method will most likely be the point-based registration method as presented by Van Doormalen et al.[76] with an additional image target for real-time tracking of the patient.

1.5 Research aim and objectives

To be able to transfer the VSP using AR several steps have to be taken. The first will be the creation of a HoloLens application which is able to register and track the patient in real-time and allows the user to accurately see and transfer the VSP onto the patient. This application will have to be user-friendly, intuitive and robust. Next, the created application will have to be validated and tested, to determine if it is possible to reach the desired 2 mm error margin. And to determine how well it performs in comparison to surgical guides, which are the current gold standard for transferring surgical planning.

Therefore, the aim of this thesis will be:

To create an accurate augmented reality application to visualize and to transfer the virtual surgical planning for open cranial vault reconstruction onto the patient

To reach this aim, the following two sub questions are drafted:

- To what extend is it possible to create an accurate and easy to use application for the HoloLens to transfer a VSP onto a patient?
- How does the created application perform in comparison to surgical guides?

1.6 Outline

In the introduction, the clinical relevance and research aim are explained. First, craniosynostosis and its treatment options are introduced, followed by an introduction to AR, specifically the HoloLens, and its current role in clinical practice. The possibility to use the HoloLens for OCVR is explored and a research aim is drafted in the last part of the introduction.

In chapter 2, the workflow for OCVR with AR implemented in it, is described. This chapter contains three parts in which the key elements are explained. The first part is data acquisition and processing(2.1), the next is patient registration and tracking(2.2) and the last is transferring of the virtual planning(2.3).

Chapter 3 continues with the application presented in the previous chapter and describes the study that was performed to determine its accuracy compared to that of surgical guides. Followed by chapter 4 wherein the results are presented.

Chapter 5 begins with the discussion of two of the major components and two issues that are not easily solvable. Followed by the interpretation of the results, why the used registration method was chosen for the study, what factors have influenced the accuracy and what the maximal measurable accuracy is. Thereafter, the steps that have to be taken to complete the clinical workflow, to implement the reconstruction phase in the application are explained and how the presented application can be used for other interventions. The discussion is finalized with the opportunities created by the introduction of the HoloLens 2. Followed by the conclusions in chapter 6. Parts of these chapters 1-6 have been submitted for publication in Scientific Reports on 22-01-2020.

The thesis is concluded with chapter 7, an article on how the created AR application can be used for a proportional condylectomy. This study was performed using the application initially created for OCVR. This article was submitted for publication in International Journal of Oral-Maxillofacial Surgery on 31-12-2019.

2. HoloLens application design

In this chapter, the workflow from CT scan to transferring the virtual planning is presented. In figure 5, a global overview is given of the three major steps in the workflow. The first step is gathering and processing of the patient's data. The second step is patient registration and tracking within the application and the last step is the transfer of the created virtual planning onto the patient. Each step is explained in more detail in the following subsections, focused on the design of the application.

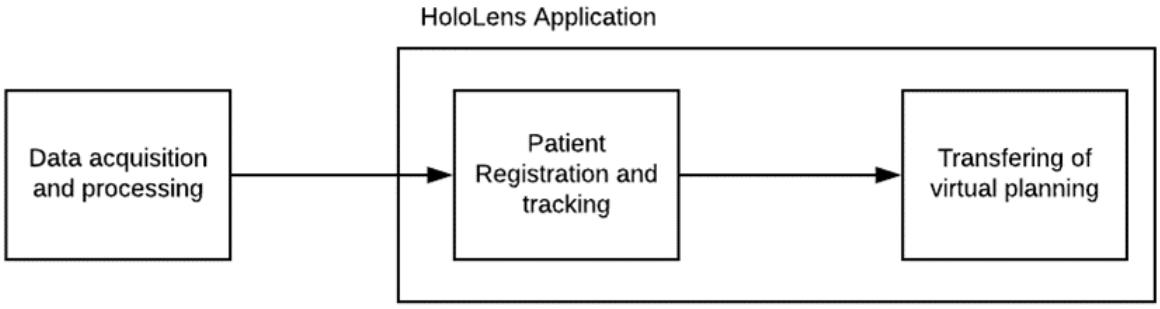

Figure 5 Overview of the workflow.

2.1 Data acquisition and processing

Data acquisition started with a CT scan of the patient, which was acquired as part of the standard protocol for craniosynostosis diagnosis. From this scan a 3D-surface mesh of the patient's skull could be derived using threshold-based segmentation. On this surface mesh of the skull, the osteotomy pattern was designed based on the type of craniosynostosis. To make transfer of the osteotomy pattern easier, it was also converted to a set of osteotomy points in the CT reference frame, ${}^{CT}\boldsymbol{q}_{\mathrm{i}}$ with $i = 1, \dots, I$. These points were placed on intersections of the osteotomy pattern and in case of osteotomy lines spanning a large distance, several points were placed in between the intersections. After transfer of these points, the pattern could be recreated by connecting the delineated points. From the created osteotomy pattern, the osteotomy guides(see section 3.1) and the reconstruction phase could also be created. The reconstruction phase consists of the created surfuces after performing osteotomy, the cranial segments. Each of these segments gets a transformation matrix containing the translation and rotation that described the transformation from the original to the new position. All the surfaces were created within the same CT reference frame (CT). The last part of data processing was the determination of registration points, ${}^{CT}\boldsymbol{p}_n$ with $n = 1, \dots, N$, on the surface mesh that would be easily recognizable in a patient. For example the supraorbital foramen, which could be used in case of trigono- and plagiochepaly patients.

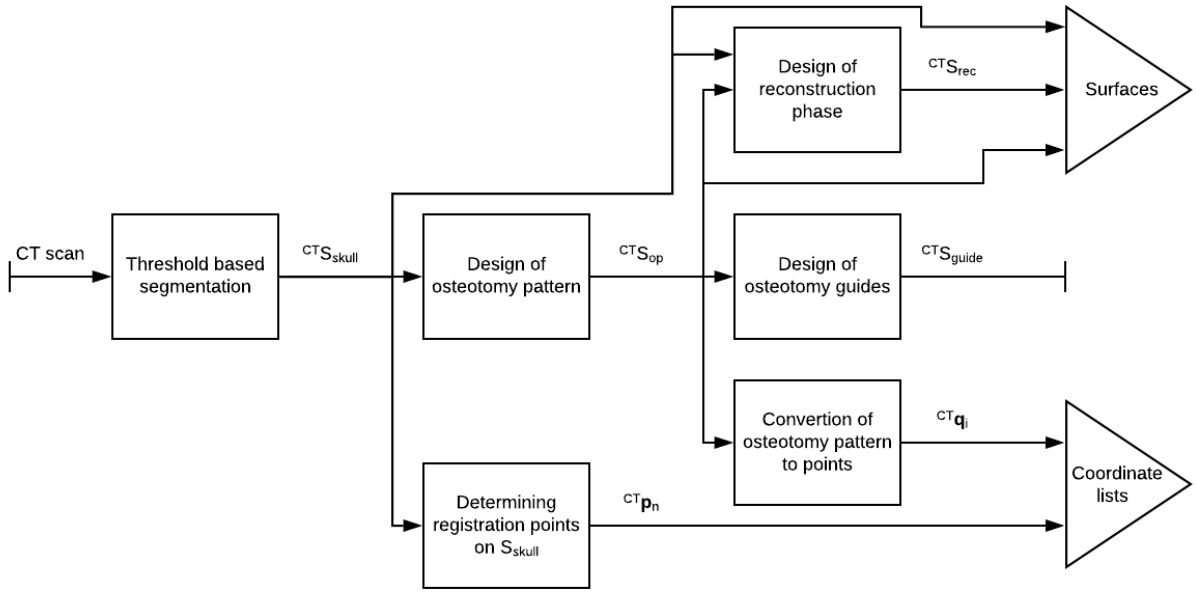

Figure 6 Flowchart of data acquisition and processing.

2.2 Patient tracking and registration

An accurate registration of the patient is required to get an accurate transfer of the VSP on to the patient. Vuforia was the chosen tracking software, because of its ability to use the HoloLens' build-in camera for real time tracking. In this study, QR codes were chosen as image targets since they had already been proven easy to use and accurate to track in earlier studies.[78] The QR codes were laser engraved on 5x5 cm medical grade stainless steel plates. Earlier experiences with Vuforia and the HoloLens showed us that size of the QR codes influence the optimal tracking distance, but not necessarily the accuracy. Since the goal was to implement the application in the OR, the optimal working distance should be around 50 cm (distance between the surgeon and the patient). The exact way how Vuforia's image tracking algorithms work are sealed off and not open to the developers who use it. They utilize a form of feature detection to recognize the QR codes and determine the orientation, position and size in the 3D space based on the size and orientation of the detected features.

Two options were available for the registration of the patient using QR codes. The easiest one to implement was placing the QR code on a known position on the patient. The link between the QR code and patient could be made in such a way, that recognition of the QR was sufficient for the correct projection of the VSP virtually attached to it. Implementation of this method will be further discussed in the Materials & Methods section of Part 2. The second method for registration of the patient was more complex and relied on an implementation of point-based registration of the patient using the QR code as reference position on the patient. Point-based registration is a method to register the patient in the

real world (HoloLens reference frame) based on known positions of landmarks in the virtual world (CT reference frame). Since one QR code is already used to continuously track the position patient, a second one was needed to register the registration points in the HoloLens reference frame. This second QR code was laser engraved on a medical grade stainless steel pointer, see figure 7. The implementation of point-based registration consisted of three steps:

1. Determining the position of the real-world registration points in the HoloLens reference frame in respect to the reference QR code.
2. Data association; to match the set of virtual registration points to the real-world registration points.
3. Determining the transformation between the HoloLens reference frame and the CT reference frame using a Procrustes algorithm.

Figure 7 Stainless steel pointer with QR-code and reference QR-code.

The implementation of the first step was done using Vuforia image tracking. The transformation matrix of both QR codes, ${}^{H}_{QR,r}T_{(t)}$ and ${}^{H}_{QR,p}T_{(t)}$, with $t = 0, \dots, T$, can be requested within the application at any given time. QR, r represents the reference QR and QR, p the pointer QR. Each matrix consists of a translation $\mathbf{p}$, rotation R and scale within the HoloLens reference frame. To get the position of the registration point, an offset was given to the QR code on the pointer to get the position of the tip of the

pointer, which can be described as ${}^{QR,p}\boldsymbol{z}_{tip}$. Using this data, the position of the registration point in the reference QR coordinate system can be determined using the following formula:

$$ {}^{QR,r}\boldsymbol{p}_n = {}^{QR,r}_{H}T_{(t)}\ {}^{H}_{QR,p}T_{(t)}\ {}^{QR,p}\boldsymbol{z}_{tip} \text{ with } {}^{QR,r}_{H}T_{(t)} = {}^{H}_{QR,r}T^{-1}_{(t)} \quad (1) $$

For easier explanation of the algorithm, the implementation of the algorithm is viewed from a static point of view where $t = 0$ and all elements are transformed to the HoloLens reference frame. Using the formula above, a set of registration points was gathered with *N* registration points in the HoloLens reference frame H. This set can be described as ${}^{H}\boldsymbol{p}_n \in \mathbb{R}^3$, with $n = 1, \dots, N$, where the set of virtual registration points in the CT reference frame (CT) can be described as ${}^{CT}\boldsymbol{p}_n \in \mathbb{R}^3$. Each point in one of the sets has an associating point in the other set. So the points in ${}^{H}\boldsymbol{p}_n$ have to be sorted so that:

$$ {}^{H}\boldsymbol{p}_1 \triangleq {}^{CT}\boldsymbol{p}_1, \dots, {}^{H}\boldsymbol{p}_n \triangleq {}^{CT}\boldsymbol{p}_n \quad (2) $$

To associate the data points in both sets, the user of the application must select the registration points in the same order as in ${}^{CT}\boldsymbol{p}_n$. To improve the user-friendliness and robustness of the application, a brute-forcing method was implemented for the data association. The method of brute-forcing creates every possible combination of ${}^{H}\boldsymbol{p}_{m(n)} \triangleq {}^{CT}\boldsymbol{p}_n$, applies the Procrustes algorithm to it and then calculates the root-mean-squared error (RMSE) for that association.

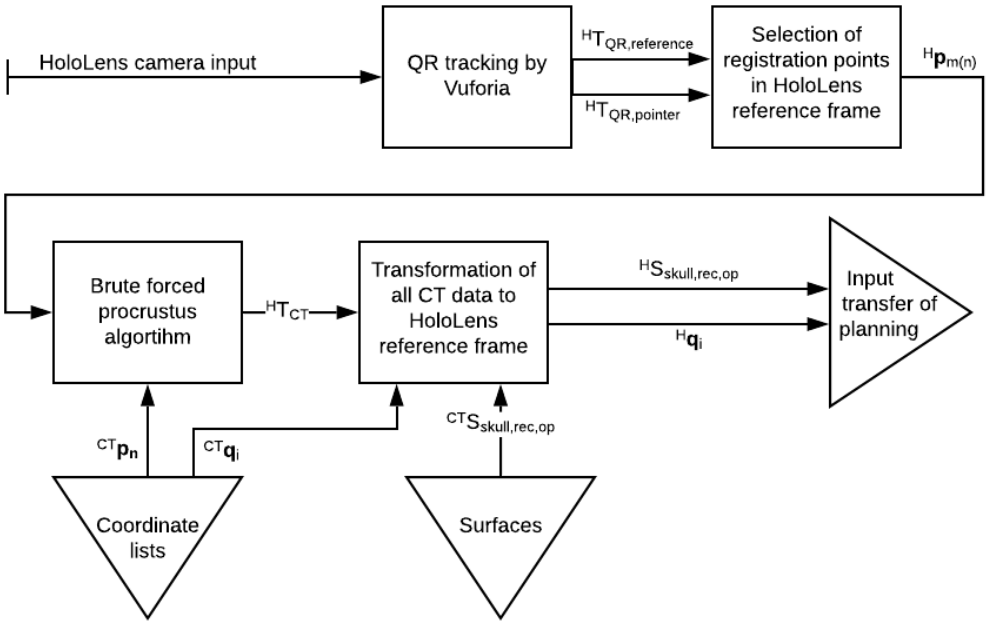

Figure 8 Flowchart of patient tracking and registration.

Next, the association order $m(n)$ with the lowest RMSE was selected. The translation ${}^{H}_{CT}\boldsymbol{t}_{j_{opt}}$ and rotation matrix ${}^{H}_{CT}\boldsymbol{R}_{j_{opt}}$ corresponding to this association order was used to translate and rotate the VSP containing ${}^{CT}S_{\,skull}$, ${}^{CT}S_{\,reconstruction}$, ${}^{CT}S_{\,osteotomypattern}$ and ${}^{CT}\boldsymbol{q}_i$ to the correct position in the HoloLens reference frame, see Formula 3. Scaling was not implemented in the application, because the scales of both reference frames are already equal. Besides applying the found transformation matrix to the VSP, it was also virtually attached to the reference QR code to ensure the VSP would stay at the correct position in respect to the patient, see Formula 4. A detailed description of this algorithm can be found in Figure 9 and an overview of the workflow can be found in Figure 8.

$$ {}^{H}\boldsymbol{q}_i = {}^{H}_{CT}\boldsymbol{R}_{j_{opt}}\,{}^{CT}\boldsymbol{q}_i + {}^{H}_{CT}\boldsymbol{t}_{j_{opt}} \tag{3} $$

$$ {}^{QR,r}\boldsymbol{q}_i = {}^{QR,r}_{H}\boldsymbol{T}_{(t)}\,{}^{H}\boldsymbol{q}_i \tag{4} $$

Input: the dataset of ${}^{H}\boldsymbol{p}_{m(n)}$ with *m* being one of the *n*! association orders in reference frame H and dataset ${}^{CT}\boldsymbol{p}_{n}$ in reference frame CT

Model: ${}^{H}\boldsymbol{p}_{n} = {}^{H}_{CT}\boldsymbol{R}\,{}^{CT}\boldsymbol{p}_{n} + {}^{H}_{CT}t$

Output: lowest RMSE and associated rotation matrix $\boldsymbol{R}$ and translation t

1. Foreach $m_j(n)$ with $j = 1, \dots, N!$ in ${}^{H}\boldsymbol{p}_{m_j(n)}$
    a. Calculate centroid of each dataset ${}^{H}\overline{\boldsymbol{p}} = \frac{1}{N}\sum_{n=1}^{N} {}^{H}\boldsymbol{p}_{j}$ and ${}^{CT}\overline{\boldsymbol{p}} = \frac{1}{N}\sum_{n=1}^{N} {}^{CT}\boldsymbol{p}_{n}$
    b. Normalize all points: ${}^{H}\widetilde{\boldsymbol{p}}_{j} = {}^{H}\boldsymbol{p}_{j} - {}^{U}\overline{\boldsymbol{p}}$ and ${}^{CT}\widetilde{\boldsymbol{p}}_{n} = {}^{CT}\boldsymbol{p}_{n} - {}^{CT}\overline{\boldsymbol{p}}$
    c. Calculate rotation matrix ${}^{H}\boldsymbol{R}_{CT}$ using SVD such that $USV^{T} = \tilde{A}\tilde{B}^{T}$, then calculate ${}^{H}_{CT}\widehat{\boldsymbol{R}}_{j} = UV^{T}$
    d. Calculate translation ${}^{H}_{CT}\hat{t}_{j} = {}^{H}\overline{\boldsymbol{p}} - {}^{H}_{CT}\widehat{\boldsymbol{R}}_{j}\,{}^{H}\overline{\boldsymbol{p}}$
    e. Apply registration ${}^{CT}\widetilde{\boldsymbol{p}}_{n} = {}^{H}_{CT}\boldsymbol{R}_{j}\,{}^{CT}\boldsymbol{p}_{n} + {}^{H}_{CT}t_{j}$
    f. Find association order m(n) with the smallest root mean squared error (RMSE)

$$RMSE_j = \left\| \sqrt{\frac{1}{N}\sum_{n=1}^{N}\left({}^{H}\boldsymbol{p}_{j} - {}^{CT}\widetilde{\boldsymbol{p}}_{n}\right)^{2}} \right\|$$

2. $j_{opt} = \underset{j=1,\dots}{\arg\min}\,(RMSE_j)$
3. $RMSE_{opt} = RMSE_{j_{opt}}$
4. ${}^{H}_{CT}\boldsymbol{R}_{opt} = {}^{H}_{CT}\boldsymbol{R}_{j_{opt}}$
5. ${}^{H}_{CT}t_{opt} = {}^{H}_{CT}t_{j_{opt}}$

Figure 9 Detailed description of Procrustus algorithm and its implementation using brute-forcing.

2.3 Transfer of virtual planning

One of the first steps for an accurate transfer of the VSP onto the patient is to make sure that the HoloLens is placed correctly on the user's head to assure his perception of the position of the VSP is correct. Next, the VSP has to be delineated onto the patient in an accurate way. For the transfer of the VSP several methods were implemented in the application.

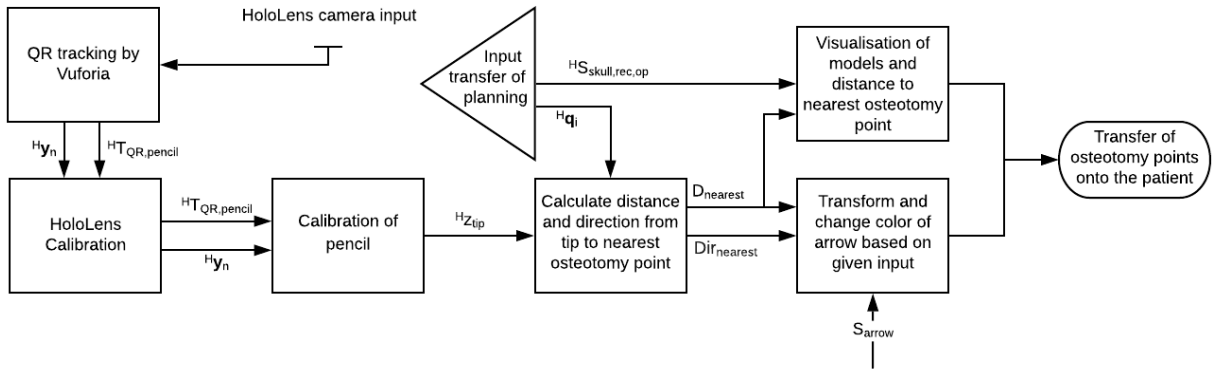

Figure 10 Flow chart of transferring of VSP onto the patient.

2.3.1 Calibration of the HoloLens

The HoloLens has a screen in front of each eye where the VSP is projected on. The projection on these screens is constantly adjusted based on the orientation and position of the HoloLens within the HoloLens coordinate system, to give the user the perception that the VSP is fixed in the virtual space. However, the HoloLens can not take into account what the position of the user's eyes is in respect to the screens. For example, if the HoloLens is placed to high on the user's head, all projection of the VSP are shown higher than they are. This applies to each direction. And thus, correct placement of the HoloLens is key to getting an accurate perception of the projected VSP. Therefore, two calibration methods were implemented in the application.

The first one was a rudimentary one, to get the user to place the HoloLens correctly on his head. For this, the pointer with the QR code on it was used. The 3D model of the pointer was added to the application and placed correctly on the corresponding QR code. Upon detection of this QR code, the 3D model of the pointer was displayed. In theory, the 3D model should be shown as an exact overlay of the physical pointer. But in reality, this is only the case when the HoloLens is placed correctly and thus the user was instructed to correct the placement of the HoloLens based on the mismatch the user saw between the physical pointer and the projected 3D model of the pointer, see Figure 11A and 11B.

The second method was created in case the user was not able to correctly place the HoloLens on his head. This method was designed virtually correct the offset caused by the misalignment of the screens. A calibration scene was added to the application for correction of the offset that could be seen between the real and virtual pointer, see Figure 11. Using different buttons for each direction, the offset could be corrected in a similar way as the first method, but without adjusting the position of the HoloLens.

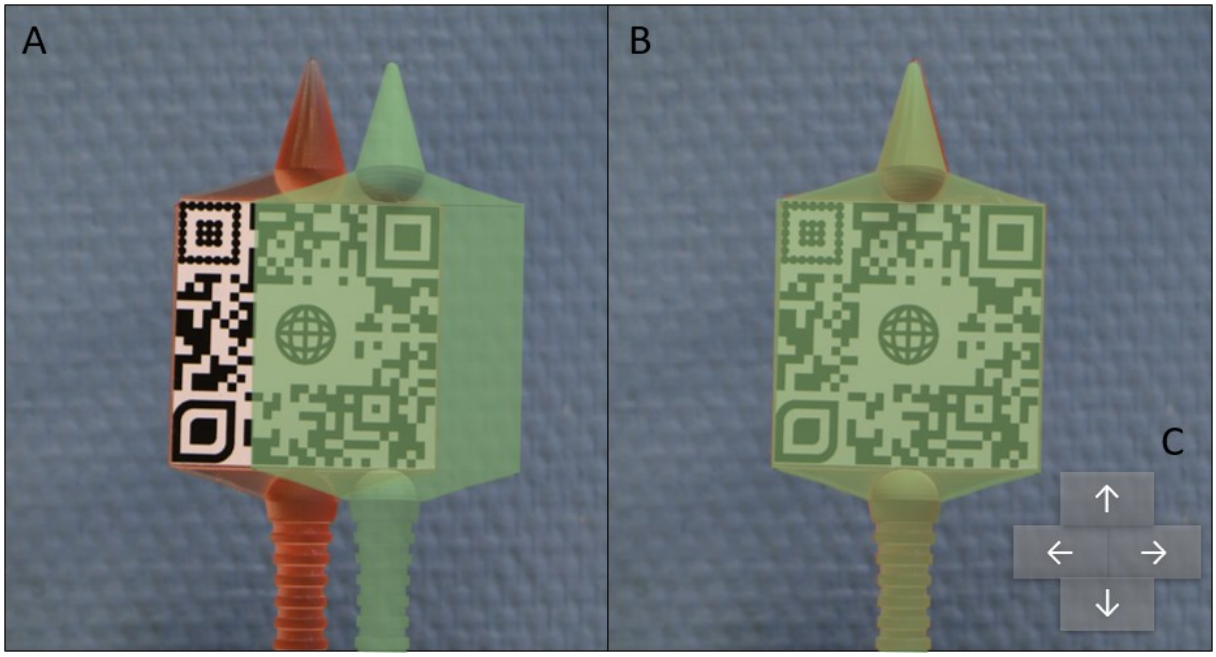

Figure 11 Two alignments of the holographic projection of the pointer over the physical pointer, where one shows a severe misalignment (A) and one show the correct alignment (B). Virtual buttons (C) were added to the application to correct the alignment.

2.3.2 Transfer of the VSP

For the actual transfer of the VSP, three different methods were developed, integrated in the application and tested. The most basic way to transfer the VSP was to directly delineate the osteotomy points as seen by the user and could be performed right after calibration and registration of the patient, the direct transfer method. The second method only used the virtual world, in which the pencil was also tracked by the HoloLens. To implement this method a QR code was made that could be attached to a pencil, after which the pencil had to be calibrated. Therefore, a calibration protocol was created wherein the reference QR code was used as calibration target. The protocol required the user to touch a corner of the reference QR code with the tip of the pencil. The positions of this corner was known and can be described as ${}^{QR,r}\boldsymbol{y}$. Using the tracked pose of the QR, ${}_{QR,pencil}{}^{H}\boldsymbol{T}_{(t)}$, and the positions of the corners, the offset between the QR code and the tip of the pencil could be calculated. This resulted in a trackable pose of the tip, ${}^{QR,pencil}\boldsymbol{z}_{tip}$, see Formula 5. After calibration a 3D model of a pencil was projected over

the actual pencil which allowed the user to focus only on the virtual world when transferring the VSP, which could make it easier to accurately transfer the VSP. This method was named the holographic transfer method.

$$^{QR,pencil}\boldsymbol{z}_{tip} = {}^{QR,pencil}_{H}\boldsymbol{T}_{(t)}\,{}^{H}_{QR,r}\boldsymbol{T}_{(t)}\,{}^{QR,r}\boldsymbol{y} \tag{5}$$

The third method, the navigated transfer method, was created based on the same idea that focusing on both the real and virtual world at the same time is difficult. However, for this method the real world was chosen to focus on. The same QR code that could be attached to a pencil was used and the same calibration protocol was implemented. However, for this method the user was instructed to transfer the VSP by focusing on the real world. To guide the user to the right position without having to focus on the virtual object, two forms of feedback were added to the application. To be able to give this feedback, the Euclidean distance,$D_{nearest}$, and a directional vector, $\vec{v}_{nearest}$, between $^{H}z_{tip}$ and all osteotomy points $^{H}q_i$ were continuously calculated.

For the first form of feedback a 3D arrow was project on the QR code. To guide the user, this arrow pointed in the direction $\vec{v}_{nearest}$ that corresponded to the smallest $D_{nearest}$. To give the user feedback on the distance between the tip of the pencil and the nearest osteotomy, it was programmed to change color the closer it was to the osteotomy point. Since the goal was to transfer the VSP with an error margin of 2 mm, the color changed from red to orange when the tip was within 4 mm of the osteotomy point and to green when the tip was within 2 mm. Besides the feedback on the QR code, $D_{nearest}$ was also displayed in the top left corner of the screens. Both forms of feedback were designed to be able to see without having to focus on it and thus allowing to user to keep his focus on the real world while tracing the osteotomy points.

In the next chapter, the three transfer methods will be tested to determine which is the most accurate and will be used in further studies.

2.4 Realization

For this thesis the Microsoft HoloLens (first version, Microsoft, Washington, USA) was used as AR device. All the surfaces were created in 3DMedX(v. 2.1, 3D Lab RadboudUMC, Nijmegen) and the 3D modelling was done using Blender (v.2.79, the Blender foundation, Amsterdam). The development of the application was done in Unity (v5.6.5, Unity Technologies, San Francisco), a cross-platform game engine that allows the user to create 2D, 3D, virtual and AR application for a wide variety of platforms. Scripting

of the application was written in C# using the integrated development environment of Microsoft Visual Studio (2019 version 16.4.0, Washington, USA). Within Unity, two software-development kit's (SDK) were used to streamline the development process. The first was the Vuforia Augmented Reality SDK (v7.1, PTC Inc. Massachusetts, USA), this SDK enables the creation of AR applications using computer vision technology recognize and track images in a 3D space in real time using the integrated camera of the HoloLens. The second SDK was the ONS SDK, an in house developed collection of code and building blocks for Unity. Making it easier for developers to transfer knowledge, creating applications with similar interfaces and interchangeable functionalities.

3. Material & Methods

Using the developed application, the accuracy and usability of the application was evaluated and compared to surgical guides which are the current gold standard for transferring surgical planning. The main goal was to determine if an error margin of <2 mm was achievable.

3.1 Study design

Ten patients who underwent an OCVR based on a VSP were included in this retrospective study. The included patient population consisted of four scaphocephaly patients, three trigonocephaly patients and three plagiocephaly patients. This study was approved by the Institutional Review Board of the Radboud University Medical Centre (no. 2019-6070). CT scans (slice thickness 0.5 mm, slice increment 0.5 mm, Aquilion ONE, TOSHIBA, Tochigi, Japan), that were acquired as part of the standard protocol for craniosynostosis treatment, were used to create 3D models of the patient's calvaria using a threshold-based segmentation in 3DMedX (v. 2.1, 3D Lab RadboudUMC, Nijmegen). On every 3D model, additional measuring beacons were appended to perform accuracy tests as described in the next section and were also used as registration points for the point-based registration.

Three-dimensional modeling software, Blender (v.2.79, the Blender foundation, XX) was used to create the VSP. The VSP included the osteotomy pattern on the intact calvaria of the patient and a 3D plan for intra-operative positioning of the newly formed cranial segments. Dissection guides with a thickness of 2 mm were designed in Blender. The dissection guides had a unique fit over the surface of the crania, but covered only the cranial part that needed to be dissected. Small recesses were made in the dissection guides at anatomical landmarks. These enabled the user to check if the dissection guides

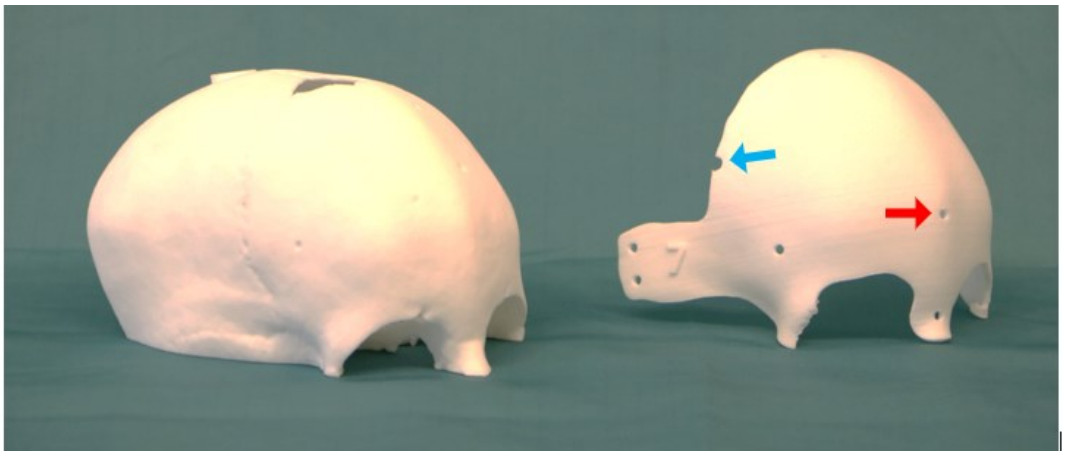

Figure 12 3D printed cranial shape of a trigonocephaly patient with surgical guide. The gaps (indicated by red arrow) were used to delineate the VSP on the patient with a pencil. Small recesses in the guide indicated an anatomical landmark (yellow arrow) to check if surgical guide was correctly positioned.

were placed correctly on the 3D models (Figure 12). A pencil was used to mark the osteotomy pattern on to the 3D shape. All 3D models and guides were 3D printed using the selective laser sintering printing technique (Oceanz, Ede, The Netherlands).

To ensure that the 3D printed skulls were reusable, all the skulls were coated with one layer of white primer and two layers of white spray paint. This created a smooth layer on the otherwise porous surface of the prints. This made it possible to wash off the delineated points of the felt tip pen, so that the observers could not see where other points had been delineated before.

3.1 Transfer method

First, the preferred transfer method had to be determined from the three implemented transfer methods. The direct transfer method, the holographic transfer method and the navigated transfer method. To determine which one was best, one observer was tasked with delineating 10 osteotomy points with each method, which were thereafter reconstructed to 3D positions and Euclidean distances to the planned positions as described in the next sections.

3.2 Improved trilateration method

For each delineated osteotomy point, a Euclidean distance to each of the beacon points was measured. This resulted in a set 5-6 Euclidean distances depending on the amount of beacon points that were placed on the skull, this set can be described as $d_{m(i)}$ with $i = 1, \dots, 10$ Euclidean distances for each beacon point M with $m = 1, \dots, M$. From these distances, a 3D position had to be reconstructed in the CT reference frame to be able to determine the error margin of each delineated point. The first method used to calculate these positions was based on the trilateration principle.[79] It uses the position of the beacon points and the measured Euclidean distances to determine the optimal position of the delineated osteotomy point. However, this method produced unexpected results. Since small measuring errors were introduced while measuring the Euclidean distances, the calculated positions floated around the actual osteotomy point. Most of them did not lie on the surface of the 3D model, which is expected when the points are delineated on a 3D print of the same model.

To overcome this problem, an improved trilateration method was developed with the constraint that the delineated points had to lie on the 3D model they were drafted on. To fulfill this constraint, the surface meshes of the 3D models were used. All vertices in a surface mesh can be regarded as dataset $\boldsymbol{x_n}$ with $\boldsymbol{N}$ vertices. Of each vertex, the distances to the beacon points in dataset $\boldsymbol{b_m}$ with M beacon points were calculated. Resulting in $D_{n,m}$ containing all Euclidean distances from each vertex to each beacon point. These distances were then compared to the measured distances $\boldsymbol{d_{m(i)}}$ and the vertex with the lowest differences was chosen as most likely position where the osteotomy point was delineated. Finally, the Euclidean distance between delineated point $\boldsymbol{c_i}$ and planned point $\boldsymbol{q_i}$ was calculated. This was done for each delineated point. See Figure 13 for a more detailed algorithm.

Input: beacon points $\boldsymbol{b_m} \in \mathbb{R}^3$, with $m = 1, \dots, M$, vertex points $\boldsymbol{x_n} \in \mathbb{R}^3$, with $n = 1, \dots, N$, measured distances $\boldsymbol{d_{m(i)}} \in \mathbb{R}^3$, and planned points $\boldsymbol{q_i}$, with $i = 1, \dots, 10$

Output: Euclidean distance E_i between calculated points $\boldsymbol{c_i}$ and planned points $\boldsymbol{q_i}$

1. For all $n = 1, \dots, N$ and for all beacons $m = 1, \dots, M$

$$D_{n,m} = \|\boldsymbol{x_n} - \boldsymbol{b_m}\|$$

2. For all $n = 1, \dots, N$ and for all planned points $i = 1, \dots, 10$

$$J_{n(i)} = \sum_{m=1}^{m} \left\| D_{n,m} - \boldsymbol{d_{m(i)}} \right\|$$

$$n_{opt(i)} = \underset{n=1,\dots,N}{\operatorname{argmin}}(J_{n(i)})$$

3. Determine the positions of the delineated points based on the found optimum

$$\boldsymbol{c_i} = \boldsymbol{x_{n_{opt(i)}}}$$

4. Calculate Euclidean distances between the calculated points and the planned points

$$E_i = \left\| \sqrt{(\boldsymbol{c_i} - \boldsymbol{q_i})^2} \right\|$$

Figure 13 Algorithm for reconstructing 3D positions and Euclidean distances to the planned points from the measured Euclidean distances.

3.3 Validation of improved trilateration method

To validate the improved trilateration method one of the skulls with a set of 10 points delineated on it was used. Of these points, the 3D positions were reconstructed using the method described above. Next, a cone beam computed tomography (CBCT) scan was acquired with small glass markers placed on the delineated points. From this scan the 3D printed skull and the glass markers were segmented using 3DMedX. These models were surface based matched on the VSP, so the coordinate system of the glass markers would be the same as those of the calculated 3D positions of the delineated osteotomy points. The Euclidean distance between the reconstructed points and the glass markers was determined.

3.4 Comparison study

To compare the surgical guides with the HoloLens, two experiments were performed. In the first experiment, two observers placed the dissection guides on the cranial shapes and delineated 10 points with a pencil on to the 10 cranial shapes. A digital caliper with 0.01 mm accuracy was used to measure the Euclidean distance between the delineated points and (at least) 5 beacon points. From these distances, the 3D position was reconstructed using the improved trilateration method. Euclidean distances between the marked points and the planned points were calculated. The observers repeated the experiment two weeks later to examine intra-observer variability.

In the second experiment, the same observers used the HoloLens application to transfer the planning. Both observers were trained in using the HoloLens. After calibration and registration, 10 holographic points were delineated with a pencil on the surface of the 3D printed cranial shapes. The experiment was repeated two weeks later by the observers. To determine the measurement error two models were measured twice after delineation of the VSP and the distances between the beacon points of all skulls were measured.

3.5 Statistical analysis

Preferred transfer method

Descriptive statistics were used to compare the accuracy of the three different transfer methods created for the HoloLens. The means and standard deviations were calculated and an Analysis of Variance(ANOVA), with a significance level of alpha = 0.95, was used to determine if the differences were significant. The method with the highest accuracy was chosen to perform the rest of the study.

Validation of improved trilateration method

Descriptive statistics were used to compare the Euclidean distances for the two measurement methods. The means and standard deviation were calculated for both methods and a Student T-test, with a significance level of alpha = 0.95, was used to determine if the differences were significant.

Surgical Guides versus HoloLens

Descriptive statistics were used to compare the different transfer methods created for the HoloLens and to used to compare the size of the error (Euclidean distance) of the two modalities. The means and standard deviations were calculated for these results and Student t-tests, with a significance level of 0.05, were used to compare the results of the surgical guide with the HoloLens. Backwards linear regression was used to determine which variables influenced the outcome the most. The Intraclass correlation coefficient (ICC) was calculated to determine consistency of the measurements. IBM SPSS Statistics version 25.0 (IBM Corp., Armonk, NY, USA) was used for all the calculations.

4. Results

4.1 Transfer method

For each of three HoloLens transfer methods, 10 Euclidean distances were calculated with the improved trilateration method. The navigated transfer method was the most accurate method with an average Euclidean distance of 2.1 ± 1.5 mm, compared to 6.4 ± 2.4 mm for the holographic transfer method and 9.8 ± 8.1 mm for the direct transfer method. The one-way ANOVA showed that the results between the three methods was significant ($p < 0.05$). An impression of the navigated transfer method is given in Figure 14.

4.2 Validation of improved trilateration method

To validate the improved trilateration method, 10 delineated points one skull were measured using that method and using glass markers in a CT scan. The improved trilateration method resulted in an average Euclidean distance from the planned point of 1.1 ± 0.5 mm, where the CT scan resulted in an average Euclidean distance of 0.8 ± 0.3 mm. However, these results were not significantly different. Proving that the improved trilateration method is comparable in accuracy.

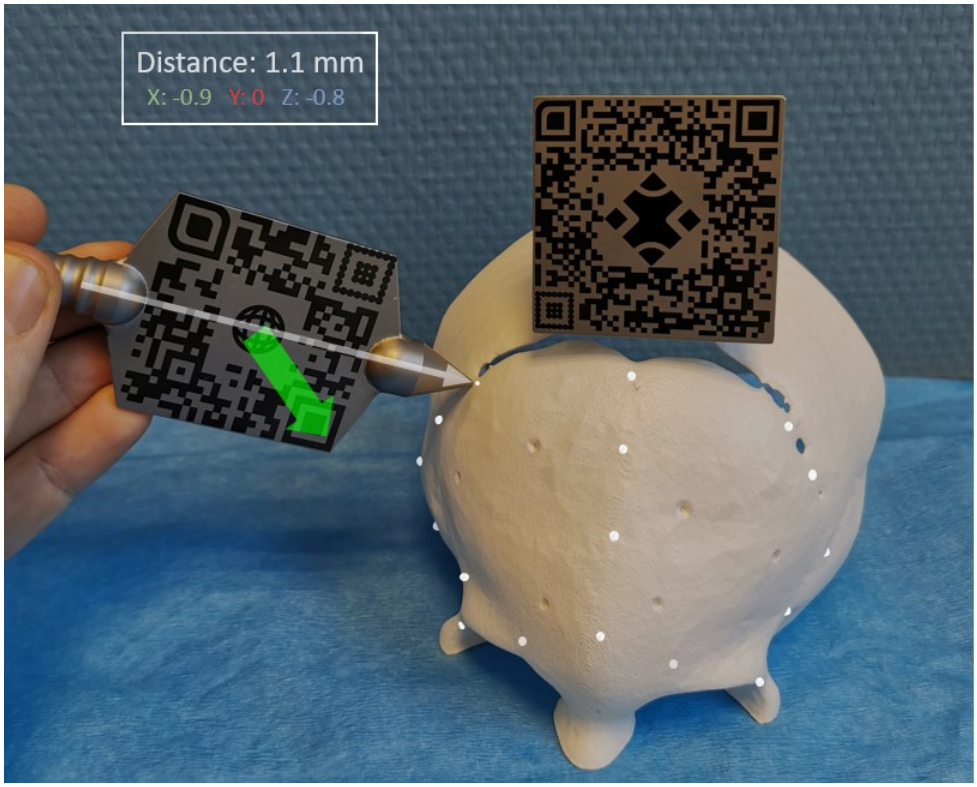

Figure 14 HoloLens application to delineate the virtual planning points on the 3D printed cranial shapes. The planning points (white) were virtually visualized on the 3D printed cranial shapes. The pointer and the pencil (equipped with an QR marker) were tracked. The green arrow in the middle of the pointer indicated how the pointer should be manipulated to target the (virtual) planned point. The distance to the target was displayed in the top left corner.

4.3 Surgical guides versus HoloLens

For each cranial shape, each moment, each modality and each observer, 10 Euclidean distances were gathered, resulting in a total of 800 measurements. Five measurements were excluded due to measuring errors. The average Euclidean distance using the surgical guide (N= 398) was 0.9 ± 0.6 mm. Distances measured using the HoloLens method (N=397) were significantly higher: 2.1 ± 1.5 mm. The average time needed to transfer the VSP using the surgical guides was 50 ± 14 seconds which was significantly lower than the time needed using the HoloLens: 8 min 24 seconds ± 2 min 54 seconds.

For both the surgical guides and the HoloLens, no significant differences were found between the measurements performed at the start of the study and two weeks later. A significant difference between observers was found for both the surgical guides and the HoloLens method indicated by the boxplots in Figure 15. Using the surgical guides, there was no significant differences in transfer time between the observers to transfer the VSP. However, there was a significant time difference between the observers when the HoloLens was used. All results are presented in Table 1.

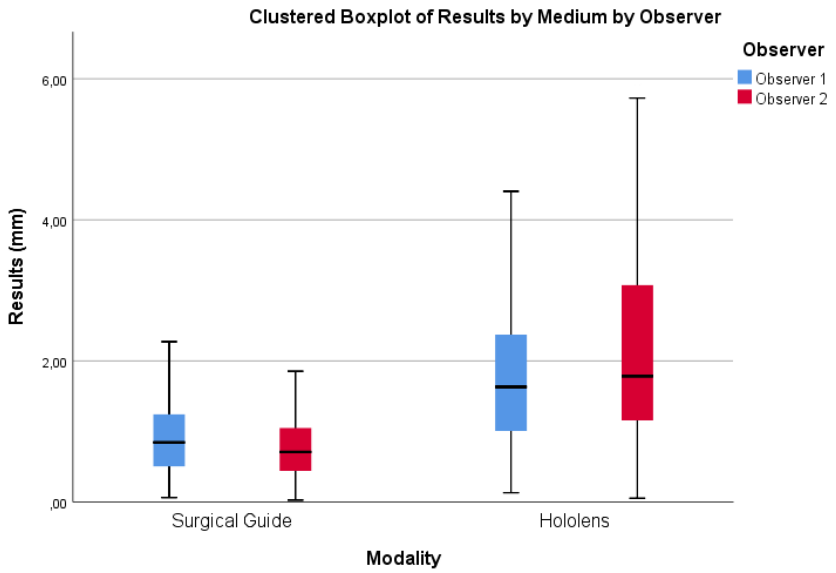

Figure 15 Boxplots of the results for both observers.

To determine which variables (transfer time, moment of performing the experiment, type of craniosynostosis, registration error and observer) influenced the outcome the most, backwards linear regression was performed on both the surgical guide and the HoloLens results. None of the variables were found to be predictors for the outcome for the surgical guides. For the HoloLens outcomes, the observer ($\beta = 0.42$, $p < 0.05$) and the RMS ($\beta = 0.979$, $p < 0.05$) were found to be predicting variables with an overall model fit of $R^2 = 0.26$.

To estimate the accuracy of the printed skulls, the distances between the beacon points were measured with a caliper. The mean difference between the measured and actual distances was 0.2 ± 0.2 mm and the Euclidean distances between calculated position of the beacon points and the actual position resulted in a mean difference of 0.4 mm.

To determine the measurement repeatability, two delineations were measured twice. No significant difference was found between the two measurements ($p > 0.05$). The absolute mean difference between the two measurements was 0.2 ± 0.1 mm, with an ICC of 1.000. The calculated positions (N=20) from these measurements also showed no significant difference ($p > 0.05$) and an ICC of 0.989.

Table 1 Results of the Surgical Guide transfer method and HoloLens transfer method

Modality	Subgroup	Variable	Mean + SD	P value
Surgical Guide	Moment	1	0.9 ± 0.5 mm	0.913
		2	0.9 ± 0.6 mm	
	Observer 1	Moment 1	0.9 ± 0.5 mm	0.377
		Moment 2	1.0 ± 0.6 mm	
	Observer 2	Moment 1	0.8 ± 0.6 mm	0.400
		Moment 2	0.8 ± 0.5 mm	
	Observer	1	0.9 ± 0.6 mm	*0.010
		2	0.8 ± 0.5 mm	
	Time	Observer 1	50 ± 14 s	0.772
		Observer 2	51 ± 14 s	
HoloLens	Moment	1	2.1 ± 1.5 mm	0.707
		2	2.0 ± 1.4 mm	
	Observer 1	Moment 1	1.8 ± 1.3 mm	0.769
		Moment 2	1.9 ± 1.0 mm	
	Observer 2	Moment 1	2.4 ± 1.7 mm	0.496
		Moment 2	2.2 ± 1.6 mm	
	Observer	1	1.9 ± 1.2 mm	*0.002
		2	2.3 ± 1.7 mm	
	Time	Observer 1	615 ± 134 s	*0.000
		Observer 2	392 ± 132 s	
	Registration error (RMS)	Observer 1	0.8 ± 0.1 mm	0.588
		Observer 2	0.9 ± 0.3 mm	

5. Discussion & Recommendations

5.1 HoloLens application

5.1.1 HoloLens calibration

One of the problems during the development of the application was calibration of the HoloLens, because incorrect alignment of the screens of the HoloLens in front of the user's eyes leads to misalignment of the VSP with the patient. This problem was also prevalent when the three transfer methods were designed and lead to development of the navigated transfer method, which also turned out to be the most accurate one. An accurate calibration makes the navigated transfer easier, but the method does not depend on it. Nevertheless, this calibration problem should be resolved to allow the use different transfer methods and usage of the HoloLens for other applications.

In the designed application, two solutions for calibration were implemented. One solution was based manual adjustment of the HoloLens to correct the position of the screens, which worked well, but was not always sufficient. Therefore, a virtual solution was also implemented to adjust the VSP to correct misplacement of the HoloLens on the user's head. This seemed to work in a setting as described in section 2.3.1, but when applied to other QR codes, the misalignment seemed to increase and depend on the orientation of the HoloLens. One thing that was not taken into account when creating this part of the application was that the orientation of the QR code influences the direction of the offset. For example, if an offset of 2 cm is given to the right, it turns into a 2 cm offset to the left when the QR code is rotated 180 degrees. And thus another method for adjusting the offset has to be developed. It should allow the user to give the projections an offset to correct the misalignment of the screens, while being independent of the orientation of the QR codes and not interfering with the tracking algorithms of Vuforia. Due to the limited time and the transfer method that was developed, which did not require a perfect overlay of the projections, this method has not been developed yet.

The HoloLens 2, expected this year, will probably solve some of the calibration issues. First of all, according to Microsoft, the fit of the HoloLens 2 is much better.[80] Making it easier for the user to correctly place the HoloLens 2 on his head and lower the need for manual corrections. And second, the HoloLens 2 has integrated eye tracking, which enables automatic adjustment of the projections based on the pupillary distance and the height of the pupils in respect to the screen.[81] The latter will most likely correct vertical misalignment. Nevertheless, research towards accurate calibration should continue.

5.1.2 Vergence-accommodation problem

The direct transfer method was the hardest to use of all the tested methods. The main reason for this is the vergence-accommodation problem which arises when the user tries to delineate the osteotomy points. Vision of humans depend on several cues to interpret 3D shapes and get a depth perception. Some of them rely on one eye, like accommodation and some rely on both eyes, like vergence. Accommodation is the process of adjusting the thickness of the lens to maintain a clear image as distance of the object focused on varies. Vergence is the process of simultaneously rotating the eyes to maintain a clear images. Normally, vergence and accommodation are linked and act as a reflex. In the case of HMD's, the eyes accommodate to the focal distance of the displays. At the same time the eyes converge to the object of interest, in this case the patient. The screens of the HoloLens are designed to have an optimal focal distance between 1.25 m and 5 m, while the patient is positioned within working distance of the surgeon at approximately 50 cm. And thus to get a clear image, the eyes have to accommodate and converge to a different distance and the vergence-accommodation problem arises.[82] This leads to double images of the holographic projections when the user tries to focus on the patient in the real world and to a blurred image of the patient when he tries to focus on the holographic projections. This makes it hard to delineate the osteotomy points directly onto the patient using the direct transfer method, because the user cannot focus on both the pencil and the osteotomy points that have to be delineated at the same time.

To overcome this problem, the navigated method was implemented in the application. Both implementations of feedback allowed the user to maintain the natural link between vergence and accommodation and lead to more comfort, sharper and less double images. Similar techniques have been described by Gao et al. who used the HoloLens for mandibular surgery.[83] These techniques turned out to be a valuable addition to the application and are part of the reason such a good accuracy was reached. Hopefully an OST-HMD will be created in the future, specifically for surgical applications, with a focal distance of 50 cm to resolve the vergence accommodation problem.

5.2 Surgical guides versus HoloLens

5.2.1 Results

As was expected, the surgical guides showed excellent results and presented an average error of 0.9 ± 0.6 mm without variation between the two test moments. Although there was a significant average difference between the observers of 0.1 mm, this difference was extremely small and not clinically relevant. In addition, only 50 seconds on average was needed to transfer the virtual planning. Only 16

out of 400 measurements showed an error larger than 2 mm which are likely caused by wrong measurement. Since the linear regression model did not reveal that any of the tested variables had a significant correlation with the outcome, we can conclude that the error was random.

With an average error of 1.9 and 2.3 mm for observer 1 and 2, the HoloLens transfer method was almost accurate enough to meet the clinical threshold of 2 mm. The outliers, and a small number of measurements with a large error, had the most effect on the results. Figure 15 shows that the median error of the HoloLens method for both observers is smaller than the mean error (1.6 and 1.8 versus 1.9 and 2.3 respectively). This means that if the outliers, and large inaccurate measurements can be eliminated, the average error and the standard deviation of the HoloLens transfer method will fundamentally improve. Errors larger than 3 mm were especially seen in the results of observer 2. Taken into consideration that observer 1 used systematically more time to transfer the VSP on the cranial shapes (10.25 minutes versus 6.5 minutes), a logical explanation is that observer 1 was more meticulous than observer 2 which resulted in fewer planning points with larger errors. To decrease this difference and increase the overall accuracy, the users of the application have to be instructed to check their delineated osteotomy points, which is possible with the navigated transfer method. If the delineation is not within the 2 mm error margin, the user can delineate the osteotomy point again.

Linear regression confirmed that the observer is the largest significant variable. However, the model fit was only 0.26, meaning that only 26% of the variation in the results can be predicted using the calculated model. Despite the weak model, we still advise the HoloLens user to be precise and take time when transferring VSP on the patient. In a clinical setting however, the extra time needed to get a more accurate transfer has to be taken into consideration, since OR time is valuable.

The registration error, expressed in RMS was second significant variable that affected the accuracy. This was expected, since the RMS is already a measure for how well the point-based registration is performed. A lower RMS means that the virtual model has a better fit over the real model. However, a better fit does not necessarily mean it is easier to get an accurate transfer, but does allow the user to get a better transfer than with a higher RMS. This is supported by the fact that the overall model fit was 0.26. This all does emphasizes that the registration is an important factor. One major benefit of AR is that the registration can be examined by the user since the landmark points or the complete 3D model can be fused with the real cranial shape and the user can inspect the registration and redo if necessary.

5.2.2 Registration method

The accuracy was better than initially expected. At the begin of this study, it was expected that HoloLens would be able to reach an accuracy of around 5 mm. Comparable to what other studies have reached.[65,66,76] The initial goal of the study was to determine the accuracy of the HoloLens itself, by reducing as many factors that could potentially induce an error. Therefore, a QR-holder was created which could be fixated in each of the printed crania and the VSP was projected based on the exact position of the QR code, similar to what Morena-Martinez et al. did with their patient specific guides.[72] However, after creating the application for this method, errors in the alignment were observed by the users. A problem that could not be resolved by improving the application or placement of the QR. Apparently, Vuforia's tracking algorithm was more sensitive than expected and small errors in the orientation of the QR code resulted in large alignment errors. These errors were caused by print inaccuracies of the QR holder, which also resulted in a loose-fit of the holder in the printed skull. To resolve this problem, point-based registration was implemented in the application, which increased the clinical relevance of the study.

To make sure that the point-based registration would not be the largest influence on the outcome, the appended beacon points were used as registration points. The exact coordinates of these beacon points were known, allowing an accurate registration of the patient. This does stress the need for meticulous selection of registration points in a clinical setting, since the achieved results will only be reproducible with an accurate registration. The registration points will have to be selected manually in a 3DCT scan, based on anatomical landmarks, such as sutures, fontanelles and foramen. Therefore, the time between the CT scan and the intervention should be reduced, to minimize the amount of growth that takes place and extra caution should be taken when creating the 3D CT scan, to minimize segmentation errors.

5.2.3 Accuracy of the measurement method

To determine a submillimeter (<1 mm) accuracy, an accurate measurement method had to be chosen. The initial technique that was investigated, was the use of 3D stereophotogrammetry. A technique that is being used extensively in the 3D Lab of the RadboudUMC. With a 3D photo accuracy of <0.2 mm, it is a good candidate for analyzing the delineations. However, to determine a Euclidean distance between the delineated point on the 3D photo and the planned position they have to be matched perfectly using surface based matching. After matching, the center point of the delineated points had to be manually determined, after which the distance could be calculated. The surface based matching introduced such large errors, that accurate determination of the delineated points was impossible. Therefore, the

improved trilateration method was created, which minimized the amount of introduced errors while determining the Euclidean distance.

To determine the accuracy of the improved trilateration method, three experiments were conducted. The first experiment showed that the measurements were extremely consistent (ICC = 1.000), with an accuracy of 0.2 mm as a result of human handling of the caliper. Subsequently, the accuracy was determined by comparing it to a more time consuming and presumably more accurate method, involving placement of glass markers on the delineated points. Even in this verification method, errors were introduced. Placement of the glass markers was done by hand, the markers themselves were 0.4 mm in diameter and in the CBCT scan, the exact position on the skull had to be manually determined, because the glass markers had to be projected back onto the surface of the skull. Nevertheless, this validation method resulted in a lower average Euclidean distance and standard deviation of 0.8 ± 0.3, compared to 1.1 ± 0.5 mm for the improved trilateration method. Even though the difference was not significant, it does suggest that the used method is an underestimation of the actual accuracy.

The last experiment that was performed was to determine the accuracy of the printed skulls, after they were coated. The distance between the beacon points was measured with the caliper and compared to what these distances were in the virtual 3D model. This showed that the printed models were slightly smaller than the virtual models, with an average difference 0.2 ± 0.2 mm.

These factors all contribute to the maximal measurable accuracy with the used methods. Taking them all into account, it is impossible to accurately determine the error margin of the transfer methods on a submillimeter level. This is also the main reason all distances presented in this thesis are rounded up to one decimal. However, this does not weaken the study results. The goal was to determine if an error margin of <2 mm was achievable, which was almost reached with the average error for both observers being 2.1 mm. Assuming that the used method gives an underestimation of the actual results, it could be stated that the HoloLens is accurate enough for the transfer of the osteotomy pattern onto the patient. However, outliers up to 8 mm were measured. This in turn, will lead to a faulty osteotomy pattern, even if the average error margin is below 2 mm. Therefore, it is recommend that follow-up research focusses more on preventing these outliers, than on improving the accuracy of the points which are already below the desired error margin.

5.3 Clinical Implementation

5.3.1 Clinical workflow

To complete the clinical workflow for AR guided OCVR, the reconstruction has to be implemented in the application and three small improvements have to be made. The first is attachment of the QR code to the patient. The QR code used in the study is sterilizable and has clearance for intraoperative use, but it was designed for deep-inferior epigastric perforator flap breast reconstructions.[78] During this procedure, there is a relatively flat surgical field on which the QR code can be placed and fixated using a transparent, sterile film. The curved surface of the skull makes it impossible to place to QR code in a similar fashion. The easiest solution to firmly attach the QR code to the skull is to attach it to a BrainLab reference star. These are already present, reusable, cleared for intraoperative use and can be firmly attached to the patient's skull. When the application proves its viability in the OR using such a makeshift QR holder, a specific QR holder can be designed which can be firmly attached to bony structures. This holder can either be a reusable device with QR laser engraved on it or a cheap disposable device in which the reusable QR code can be placed.

Thereafter, the osteotomy points have to be delineated. However, there is no QR code yet, that can be easily attached to a surgical marker. As a temporary solution, the pencil can be attached to the pointer (see Figure 17). This has been tested, but the usability was suboptimal due to the weight and shape of the pointer. For optimal results, a new sterilizable device with a QR code on it has to be created, that can easily be attached to and detached from the surgical marker.

The last improvement that can be easily implemented is addition of small indents on the corner of the QR code on which the pencil has to be calibrated. During the study, the corners were not always clear and the observers experienced problems with placing the tip of the pencil exactly at the corner of the QR code while calibrating. These indents enable exact placement of the tip of the pencil on the corner of the QR, this will lead to a more accurate and consistent calibration. Which will lead to a more accurate transfer of the VSP.

5.3.2 VSP

The VSP as consist out of 2 steps: a delineation phase and a reconstruction phase. The accuracy study only focused on the first phase, because this determines the shape of the cranial segments needed for the reconstruction phase and is therefore crucial for an adequate result. In addition, this step is more applicable for conducting accuracy tests and comparing the two transfer methods with each other. Since

the methodology of calibrating, registration and tracking is identical for both phases, similar results can be expected during the reconstruction phase. However, the reconstruction phase has not been tested yet. In the design process of the application, the steps that are taking in the reconstruction phase are implemented and visualized. Allowing the surgeon to see all steps in the reconstruction phase and get a correct view of the position and orientation of the created cranial segments, but the position and orientation can not be verified using a calibrated tool like in the delineation phase.

To get this needed verification, a method has been conceptualized that has not been implemented in the application yet. The method is based on the work of Garcia-Mato et al, they created a similar workflow for craniosynostosis surgery using a VSP, combining printed guides and AR. They did not implement real-time tracking in their application, but instead, they placed resorbable screws in the skull. After registration of the patients using anatomical landmarks, they registered these screws as a secondary set of registration points, to be used during the reconstruction phase to register the patient again. Since they did not immobilize the patient's skull during surgery, this registration step had to be used several times.[84] This gave us the idea for a verification method, these resorbable screws could also be placed in the created cranial segments. By registering these screws before the osteotomy, their position in the original skull in the VSP can be determined. Next, the position of these screws can be transformed just like the cranial segment they are placed in, to determine what their position should be after reconstruction. With this information, the verification step can be implemented in a similar fashion as the delineation phase. The user could then position the tip of the pointer on one of the screws and get feedback on the distance to the planned position by seeing the actual distance and with the same indication arrow.

5.3.3 Other implementations

The performed study showed promising results for the use of AR for the transfer of surgical planning. However, the higher transfer time and an accuracy of just above 2 mm do not make it a good alternative for surgical guides yet. Nonetheless, there are types of surgery where there is not such an open surgical field which allows the surgeons to use surgical guides. An example of such an intervention is a condylectomy, where the surgical field is small and the bone of interest cannot be exposed enough to utilize surgical guides. In such cases, the HoloLens could be an easy solution for the transfer of a surgical planning. In Part 2, implementation of the created HoloLens application for a proportional condylectomy is presented.

Easy implementation in other fields was possible, because the application was made out of building-blocks that are interchangeable with other applications. This allowed for the easy adjustments needed to use the HoloLens to guide a proportional condylectomy. To enable the further development of HoloLens applications at our department, the created building blocks will have to be integrated in the ONS SDK that was used to develop the application. This will allow other researchers and developers, to make more advanced applications in less time and will create more opportunities for the use of the HoloLens in clinical practice.

5.4 HoloLens 2

The HoloLens 2 is expected this year. It is supposed to be more intuitive and comfortable and has a better field of view and camera. Hopefully, these improvements will lead to easier, faster and more accurate transfer of VSP's even by less experienced HoloLens users. Therefore, it is recommend to prepare the created application for the arrival of the HoloLens 2. Once this is done, the HoloLens part of the performed study should be performed again to analyse the increase in accuracy and possible decrease in transfer time. Since the HoloLens 2 is supposed to be more intuitive and user-friendly, less experienced users should be included in this new study, to determine the learning curve for using the HoloLens and the application.

In the HoloLens 2, a more advanced form of hand tracking is implemented, making it much more intuitive, by allowing a more realistic way of touching, grabbing and moving virtual objects.[85] Eye tracking is also introduced, which allows the user to select virtual objects or buttons by looking at them.[81] This will open up new opportunities for the use of AR. Instead of just using the HoloLens to transfer the VSP, the entire VSP could be created inside the virtual world. All the involved surgeons and technical physicians can wear a HoloLens, which are linked together so they see the same virtual world in which the VSP will be created. The 3D model of the patient is visualized and using the more intuitive interactions, the osteotomy pattern can be drawn on the skull with ones finger. After which the application automatically creates the cranial segments. Thereafter, the optimal way to reconstruct cranial vault can be found by just grabbing the cranial segments, rotating and moving them to the desired position, until the optimal result is reached. To further improve the AR experience, haptic feedback can also be introduced[86], allowing the surgeons to actually feel the skull when they draw on it or to feel the cranial segment when they grab it. Allowing the team to virtually perform the surgery in a realistic way and letting them explore all the possibilities for the OCVR in 3D, before the actual surgery. And potentially revolutionizing the way VSP's are created and used.

6. Conclusion

To conclude, AR was explored as a new visualization technique for the transfer of VSP's for OCVR. AR enabled the use of the VSP's to their full extend, by allowing accurate visualization of the osteotomy pattern and the reconstruction phase. The created application was not able to outperform the surgical guides, both in transfer time and transfer accuracy. Nevertheless, the AR workflow showed promising results and is a potential alternative for surgical guides and navigation. Research on the implementation of AR for OCVR will have to focus on preventing outliers to get a perfect transfer of the osteotomy pattern within the error margin and on the implementation of the reconstruction phase to use AR for the entire procedure. Other possible implementations in the field of CMF surgery should be explored and new innovations, like haptic feed back, should be implemented to improve the AR experience.

Part 2

Augmented Reality guided condylectomy

Abstract

Condylectomy is frequently performed to stop the active growth in cases of unilateral condylar hyperplasia and to enhance the symmetry of an asymmetric mandible. The optimal height and position of the condylar osteotomy line can be planned by using a 3D virtual skull model based on a cone beam computed tomography (CBCT) scan. it is challenging to transfer the 3D virtual planned condylectomy accurately to the patient due to the limited surgical access and the depth of the surgical field. The use of surgical guides is in majority of cases not possible. Augment reality (AR) can aid condylectomy by presenting images of 3D virtual surgical planning on the condylar head. A new clinical workflow that uses AR in form of Microsoft HoloLens to assist a condylectomy is presented step-by-step in this study. Postoperative analysis has shown that AR-assisted condylectomy is feasible, accurate and has the potential to be implemented in the clinical setting routinely in the near future.

7.1 Introduction

Unilateral condylar hyperplasia (UCH) is a rare disorder of progressive nature and is characterized by alterations to facial function and aesthetics. [87,88] UCH is caused by an overactive growth activity in one of the mandibular condyles, but its aetiology is still uncertain and is probably multifactorial.[89] Different interventions can be used to optimize the occlusion and facial symmetry. Treatment options include a high-condylectomy, proportional condylectomy or orthognathic surgery. A high condylectomy is aimed to remove the cranial part of the condyle where the active growth centre is located, whereas a proportional condylectomy has the purpose of enhancing the symmetry of the mandible and occlusal plane by locating the height of the osteotomy line in such a way that the ramus height of the affected side matches the non-affected side.

Recently, Niño-Sandoval et al. reported in a systematic review that a proportional condylectomy is the treatment of choice to deal with active and constant growth of the condyle. [90] In addition, proportional condylectomy can be used as an initial treatment instead of a high condylectomy to avoid secondary corrective surgeries in active condylar hyperplasia. [91]

The optimal height and position of the condylar osteotomy line can be planned by using a 3D reconstructed virtual skull model based on a CBCT scan. However, it remains challenging to transfer this virtual planning to the patient during surgery. The limited pre-auricular incision and the axial location of the condylar head hamper a clear vision of the condyle, which makes it difficult to locate the planned osteotomy line. In addition, the seating of the condyle in the fossa often restricts a complete overview of the condylar head. The unfavourable size and location of the surgical field impede the use of customized surgical guides to locate the planned condylectomy plane.

The implementation of AR can aid surgical interventions by presenting images of 3D virtual surgical planning on the operation field. By using AR, the 3D planned location of the condylectomy plane can be visualized directly on the condyle. The Microsoft HoloLens is an AR-glass (head-mounted display) that projects virtual 3D holograms onto the field of view of the surgeon. The Hololens has been used for various surgical procedures [64,65,72,77,92] . The aim of this study is to present a novel AR-guided work-flow to perform condylectomy based on the 3D virtual planning.

7.2 Material & Method

Patient information was anonymized and de-identified prior to analysis. Informed consent was obtained from the patient. This study was approved by the Institutional Review Board of the Radboud University Medical Centre.

A 38-year-old female presented at the RadboudUMC with a persistent pain in the region of her left condyle. Visual inspection showed a chin point deviation to the right. A NaF^{18} positron emission tomography (PET) scan was acquired which confirmed persisting condylar growth on the left side. To treat this unilateral condylar hyperplasia, a proportional condylectomy of the left condyle was proposed.

A threshold-based segmentation in IPS CaseDesigner (KLS Martin Group, Tuttlingen Germany) was used to create a 3D model of the mandible from an extended-height CBCT scan (FOV, 16 × 22 cm; scanning time, 2 × 20 s; voxel size, 0.4 mm; 3D Imaging System, Imaging Sciences International Inc, Hatfield, PA, USA). An intraoral scans of the participant's lower dentition was acquired with the TRIOS® 3D intraoral scanner (POD TRIOS® 3, 3Shape™, Copenhagen, Denmark; software version: TRIOS 2015–1) and the dental model was registered onto the 3D model using IPS CaseDesigner. Both scans were acquired as part of the standard preoperative condylectomy protocol. From the most cranial point of the condyle, the left and right ramus height was measured on the 3D model. The optimal osteotomy plane was virtually planned in such a way that the discrepancy between the left and right ramus length was resolved.

Surgery was performed under general anesthesia with nasotracheal intubation. The condylectomy of the left condyle started with a post-tragal incision with limited superior preauricular extension through the cutis and subcutis until the lateral articular capsule was reached. This was opened through a limited horizontal incision approximately 6 mm below the zygomatic arch to gain access to the inferior joint cavity, and subsequently access to the condylar head. The surgeon identified the plane of condylectomy based on the 3D virtual planning visually. With AR, the position of this plane was checked using the following steps.

First, a sterile dental splint with a tight and unique fit was placed on the lower dentition of the patient, to which a sterile QR marker was attached (Figure 16A). The Microsoft HoloLens (Microsoft, Washington, USA) was able to determine the position and orientation of this QR marker, and thus track the position of the mandible, even during its articulating movement.

Subsequently, a stainless steel pointer, equipped with a second QR marker was used to check the location of the planned osteotomy line (Figure 16). To reach the relatively deeply located condylar surface through the limited surgical incision, the pointer was extended with a Kirschner wire.

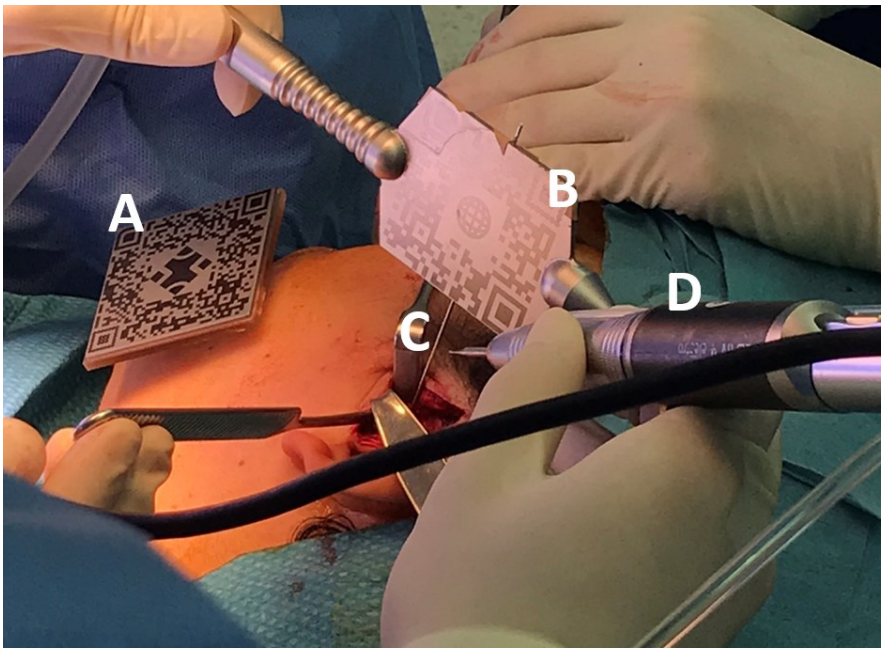

Figure 16 The mandible was tracked by the QR marker fixated on the lower dentition (A). The position of the pointer with laser engraved QR-marker (B) was tracked by the HoloLens and the tip of the Kirschner wire (C) was visualized by the surgeon in the HoloLens. The surgical drill (D) was used to perform the condylectomy.

An inhouse HoloLens application was developed that enabled the surgeon to visualize the 3D virtual planned position of the osteotomy line after gaining access to the condylar head during surgery. The HoloLens displayed a virtual arrow on the pointer that showed the surgeon how the pointer should be displaced to target the tip of the Kirschner wire on the condyle. The red color of the virtual arrow turned green in case the offset between the planned position of guidance points (on the osteotomy line) and real-time position of the tip of the Kirschner wire was below 2 mm. In addition, the absolute distance between the Kirschner wire tip and the planned osteotomy point was indicated on the top left view of the surgeon (Figure 17). In this way, guidance was provided to the surgeon by a direct and intuitive visualization of the planned position and guidance of the pointer. In this way, the surgeon was able to steer the tip of the Kirschner wire to the planned points on the lateral side of the condyle (Figure 16). The surgeon used a small round bur to mark this position on the condylar surface. Three marking points were placed on the condylar surface in this way, to indicate the plane of the condylectomy. The actual condylectomy was subsequently performed with a round bur and the cranial part of the condylar head was removed. After hemostasis with electrocautery, the articular disc and capsule were sutured and the incision was closed in layers. The patient was discharged a day after surgery and the postoperative recovery was uneventful. Five day following surgery, a postoperative check-up CBCT was acquired. A 3D

model of the mandible was rendered from this CBCT scan and surface-based registration was performed to register the postoperative mandible on the preoperative 3D virtual mandibular model and virtual surgical planning. The planned and actual location of the condylectomy planes were compared to evaluate the accuracy of the AR-guided surgery.

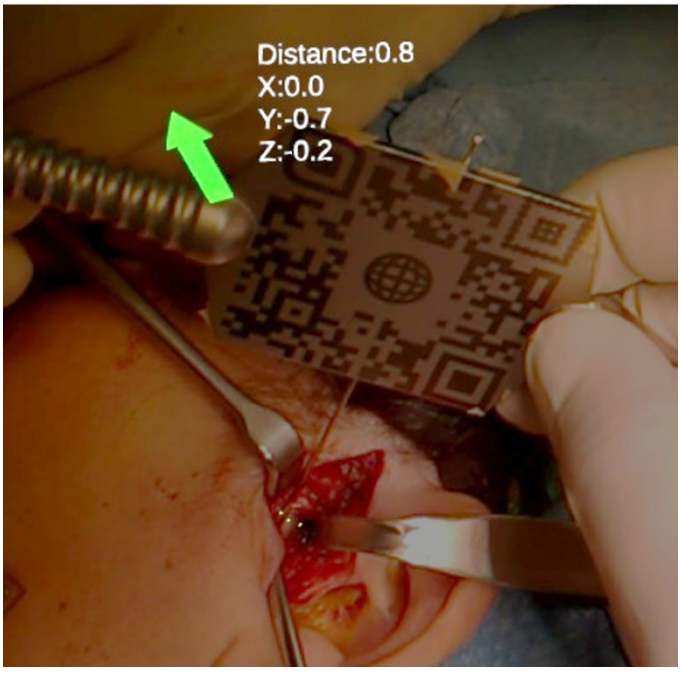

Figure 17 Visualization in the HoloLens: the green arrow indicates how the tip of the pointer should be manipulated to target the planned osteotomy position.

7.3 Results & Discussion

7.3.1 Results

The 3D registration of planned and postoperative mandibular models (Figure 18) showed that on the lateral, anterior and medial side of the condyle, the condylectomy was performed almost exactly as was planned (error ≤ 1 mm). However, the postoperative posterior border of the left condyle was located somewhat more caudally compared to the planning. This discrepancy indicated that although the starting position was well-marked, the condylectomy plane was pointed more downwards than the planning as the bur proceeded medially. This slight misalignment could be a result of the fact that only the lateral position of the osteotomy was verified by the HoloLens. Therefore, the direction of the osteotomy should be implemented in the AR-application to limit the offset on the other sides of the condyle.

7.3.2 Splint

The high quality intra-oral scan and accurate 3D printing resulted in a dental splint with a tight and unique fit on the dentition of the patient. Since the QR markers was attached, a registration process alike the point-based registration for OCVR. The virtual content could be visualized directly in the correct 3D position and orientation. This contributed to a fast and accurate workflow.

7.3.3 Future perspectives

The accuracy of the presented method should be further investigated in future research. Besides, the software can be improved to make the AR application even more intuitive. In this first step, a pointer was used to verify the planned position before the bur was used to create the osteotomy. The next step should be to equip the surgical handpiece (and thus the bur) directly with a QR code. In that way, the pointer is not required which makes the process even more intuitive to use and frees up additional space in the small surgical field. In addition, this will facilitate the guidance of the direction during the osteotomy.

Although conventional surgical navigation systems can be used to guide to user during surgery, the combination of the HoloLens with sterilizable QR markers is an easy and low-cost alternative. In addition, this AR solution allows the user to stay focused on the surgical field while attaining feedback from the planning. The surgeon is not forced to switch his or her view to an external monitor where conventional navigation data is normally displayed. [68]

7.4 Conclusion

Therefore, we believe that AR guidance is an adequate method to transfer a virtual planning for various CMF procedures. Especially during proportional condylectomy, where surgical guides are impractical, AR guidance is an effective method to assist the surgeon.

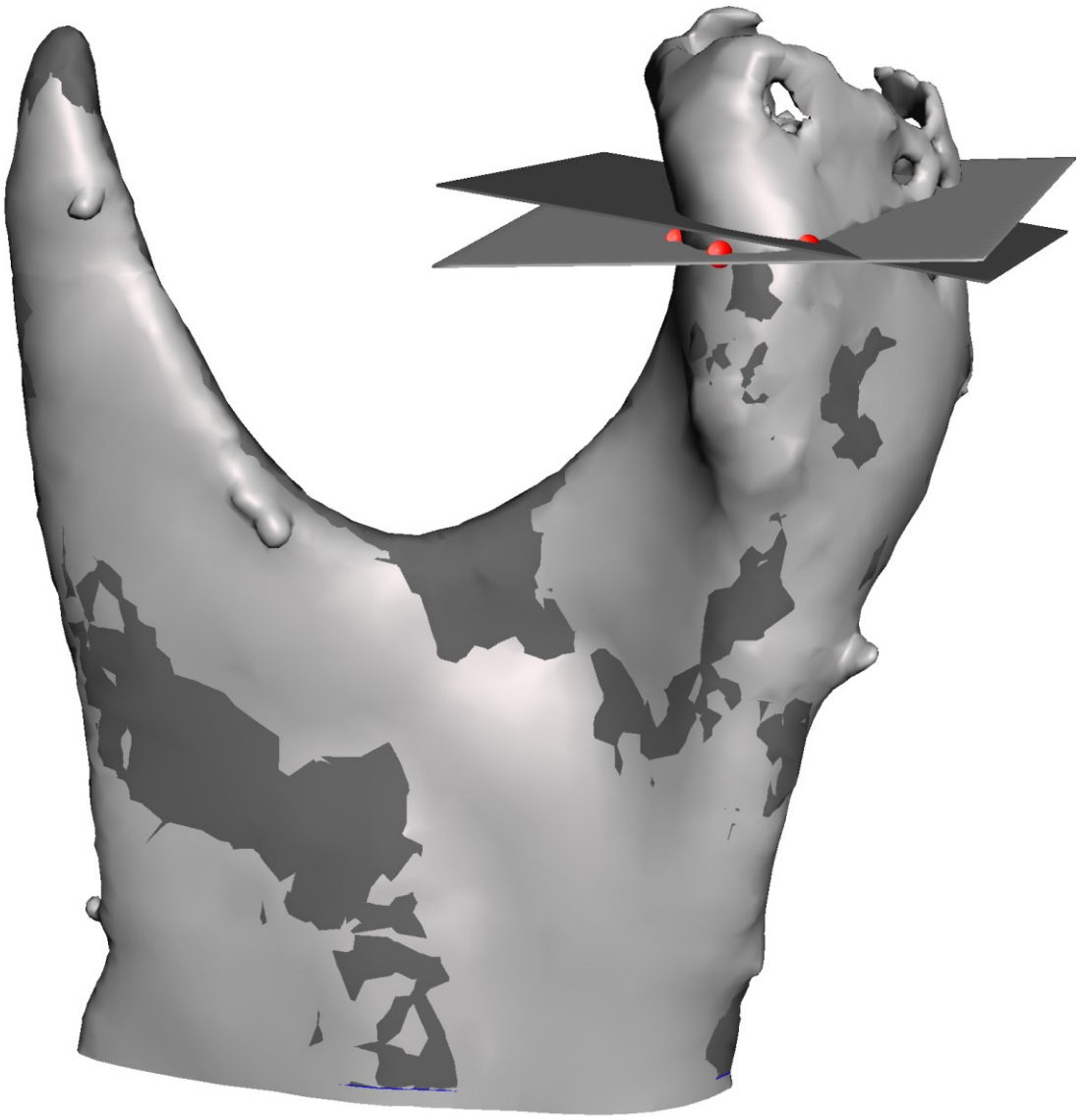

Figure 18 Lateral view of the preoperative (light gray) and postoperative (dark gray) condyle with the planned and the achieved osteotomy planes. The three points (red) were projected by the HoloLens and indicated the osteotomy plane. The posterior point was concordant with the planning and the middle point deviated by 1 mm.

References

1. T.W.Sadler. Langman's Medical Embryology Twelth Edition. *Langman's Med. Embryol.* **1**, 225–227 (2012).
2. Dekaban, A. S. & Sadowsky, D. Changes in brain weights during the span of human life: Relation of brain weights to body heights and body weights. *Ann. Neurol.* **4**, 345–356 (1978).
3. Persing, J. A., Jane, J. A. & Shaffrey, M. Virchow and the Pathogenesis of Craniosynostosis: A Translation of His Original Work. *Plast. Reconstr. Surg.* **83**, (1989).
4. Kweldam, C. F., van der Vlugt, J. J. & van der Meulen, J. J. N. M. The incidence of craniosynostosis in the Netherlands, 1997–2007. *J. Plast. Reconstr. Aesthetic Surg.* **64**, 583–588 (2011).
5. Meulen, J. Van Der *et al.* The Increase of Metopic Synostosis : A Pan-European Observation. **20**, 283–286 (2009).
6. Sá, C., Fonteles, R., Finnell, R. H., George, T. M. & Harshbarger, R. J. Craniosynostosis : current conceptions and misconceptions. **3**, 99–129 (2016).
7. Zakhary, G. M., Montes, D. M., Woerner, J. E., Notarianni, C. & Ghali, G. E. Surgical correction of craniosynostosis. A review of 100 cases. *J. Cranio-Maxillofacial Surg.* **42**, 1684–1691 (2014).
8. Governale, L. S. Craniosynostosis. *Pediatr. Neurol.* **53**, 394–401 (2015).
9. Renier, D., Sainte-Rose, C., Marchac, D. & Hirsch, J. F. Intracranial pressure in craniostenosis. *J. Neurosurg.* **57**, 370–372 (1982).
10. Starr, J. R. *et al.* Multicenter study of neurodevelopment in 3-year-old children with and without single-suture craniosynostosis. *Arch. Pediatr. Adolesc. Med.* **166**, 536–542 (2012).
11. Kapp-Simon, K. A., Speltz, M. L., Cunningham, M. L., Patel, P. K. & Tomita, T. Neurodevelopment of children with single suture craniosynostosis: A review. *Child's Nerv. Syst.* **23**, 269–281 (2007).
12. Speltz, M. L. *et al.* Neurodevelopment of infants with single-suture craniosynostosis: presurgery comparisons with case-matched controls. *Plast. Reconstr. Surg.* **119**, 1874–1881 (2007).
13. Becker, D. B. *et al.* Speech, cognitive, and behavioral outcomes in nonsyndromic craniosynostosis. *Plast. Reconstr. Surg.* **116**, 400–407 (2005).
14. Buchanan, E. P. & Hollier, L. H. Overview of Craniosynostosis. in *UpToDate* (ed. TePas, E.) (2019).
15. Mouradian, W. E. Controversies in the Diagnosis and Management of Craniosynostosis: A Panel Discussion. *Cleft Palate-Craniofacial J.* **35**, 190–193 (1998).
16. Czerwinski, M., Kolar, J. C. & Fearon, J. A. Complex craniosynostosis. *Plast. Reconstr. Surg.* **128**, 955–961 (2011).
17. Sarnat, H. B. B. T.-H. of C. N. Disorders of segmentation of the neural tube: Chiari malformations. in *Malformations of the Nervous System* vol. 87 89–103 (Elsevier, 2007).
18. Lee, B. S. *et al.* Management options of non-syndromic sagittal craniosynostosis. *J. Clin. Neurosci.* **39**, 28–34 (2017).
19. Spruijt, B. *et al.* Algorithm for the management of intracranial hypertension in children with syndromic craniosynostosis. *Plast. Reconstr. Surg.* **136**, 331–340 (2015).
20. Bir, S. C., Ambekar, S., Notarianni, C. & Nanda, A. Odilon Marc Lannelongue (1840–1911) and strip craniectomy for craniosynostosis. *Neurosurg. Focus FOC* **36**, E16 (2014).
21. Shillito, J. & Matson, D. D. CRANIOSYNOSTOSIS: A REVIEW OF 519 SURGICAL PATIENTS. *Pediatrics*

41, 829 LP – 853 (1968).

22. Delye, H. H. K. *et al.* Endoscopically assisted craniosynostosis surgery (EACS): The craniofacial team Nijmegen experience. *J. Cranio-Maxillofacial Surg.* **44**, 1029–1036 (2016).

23. Barone, C. M. & Jimenez, D. F. Endoscopic Craniectomy for Early Correction of Craniosynostosis. *Plast. Reconstr. Surg.* **104**, (1999).

24. Jimenez, D. F. & Barone, C. M. Endoscopic craniectomy for early surgical correction of sagittal craniosynostosis. *J. Neurosurg.* **88**, 77–81 (1998).

25. Proctor, M. R. Endoscopic craniosynostosis repair. *Transl. Pediatr.* **3**, 247–258 (2014).

26. Proctor, M. R. & Meara, J. G. A review of the management of single-suture craniosynostosis, past, present, and future. **24**, 622–631 (2019).

27. Jimenez, D. F., Barone, C. M. & McGee, M. E. Design and care of helmets in postoperative craniosynostosis patients: Our personal approach. *Clin. Plast. Surg.* **31**, 481–487 (2004).

28. Doumit, G. D., Papay, F. A., Moores, N. & Zins, J. E. Management of Sagittal Synostosis. *J. Craniofac. Surg.* **25**, 1260–1265 (2014).

29. Braun, T. L., Eisemann, B. S., Olorunnipa, O., Buchanan, E. P. & Monson, L. A. Safety outcomes in endoscopic versus open repair of metopic craniosynostosis. *J. Craniofac. Surg.* **29**, 856–860 (2018).

30. Chan, J. W. H. *et al.* Endoscope-Assisted Versus Open Repair of Craniosynostosis. *J. Craniofac. Surg.* **24**, 170–174 (2013).

31. Vogel, T. W. *et al.* A comparison of costs associated with endoscope-assisted craniectomy versus open cranial vault repair for infants with sagittal synostosis. *J. Neurosurg. Pediatr.* **13**, 324–331 (2014).

32. Riordan, C. P. *et al.* Minimally Invasive Endoscopic Surgery for Infantile Craniosynostosis: A Longitudinal Cohort Study. *J. Pediatr.* **216**, 142-149.e2 (2020).

33. Delye, H. K., Borstlap, W. & van Lindert, E. Endoscopy-assisted craniosynostosis surgery followed by helmet therapy. *Surg. Neurol. Int.* **9**, 59 (2018).

34. Arts, S., Delye, H. & Van Lindert, E. J. Intraoperative and postoperative complications in the surgical treatment of craniosynostosis: Minimally invasive versus open surgical procedures. *J. Neurosurg. Pediatr.* **21**, 112–118 (2018).

35. Ore, C. L. D. *et al.* Endoscopic surgery for nonsyndromic craniosynostosis: A 16-year single-center experience. *J. Neurosurg. Pediatr.* **22**, 335–343 (2018).

36. Keshavarzi, S. *et al.* Variations of endoscopic and open repair of metopic craniosynostosis. *J. Craniofac. Surg.* **20**, 1439–1444 (2009).

37. Taylor, J. A. *et al.* A critical evaluation of long-term aesthetic outcomes of fronto-orbital advancement and cranial vault remodeling in nonsyndromic unicoronal craniosynostosis. *Plast. Reconstr. Surg.* **135**, 220–231 (2015).

38. Steinbacher, D. M. Three-Dimensional Analysis and Surgical Planning in Craniomaxillofacial Surgery. *J. Oral Maxillofac. Surg.* **73**, S40–S56 (2015).

39. Chim, H., Wetjen, N. & Mardini, S. Virtual Surgical Planning in Craniofacial Surgery. *Semin. Plast. Surg.* **28**, 150–158 (2014).

40. Macmillan, A. *et al.* Virtual Surgical Planning for Correction of Delayed Presentation Scaphocephaly Using a Modified Melbourne Technique. *J. Craniofac. Surg.* **29**, 914–919 (2018).

41. LoPresti, M., Daniels, B., Buchanan, E. P., Monson, L. & Lam, S. Virtual surgical planning and 3D printing in repeat calvarial vault reconstruction for craniosynostosis: technical note. *J. Neurosurg. Pediatr.* **19**, 490–494 (2017).

42. Andrew, T. W. *et al.* Virtual Surgical Planning Decreases Operative Time for Isolated Single Suture and Multi-suture Craniosynostosis Repair. *Plast. Reconstr. Surg. - Glob. Open* **6**, e2038 (2018).

43. Shah, A., Patel, A. & Steinbacher, D. M. Simulated Frontoorbital Advancement and Intraoperative Templates Enhance Reproducibility in Craniosynostosis. *Plast. Reconstr. Surg.* **129**, 1011e-1012e (2012).

44. Khechoyan, D. Y. *et al.* Surgical outcomes in craniosynostosis reconstruction: The use of prefabricated templates in cranial vault remodelling. *J. Plast. Reconstr. Aesthetic Surg.* **67**, 9–16 (2014).

45. Soleman, J., Thieringer, F., Beinemann, J., Kunz, C. & Guzman, R. Computer-assisted virtual planning and surgical template fabrication for frontoorbital advancement. *Neurosurg. Focus* **38**, E5 (2015).

46. Pappa, H., Richardson, D., Webb, A. A. C. & May, P. Individualized Template-Guided Remodeling of the Fronto-Orbital Bandeau in Craniosynostosis Corrective Surgery. *J. Craniofac. Surg.* **20**, 178–179 (2009).

47. Queiros, C. *et al.* Use of cutting guides during craniosynostosis sequelae surgery: A comparative study between computer-assisted planning and post-operative results. *J. Cranio-Maxillofacial Surg.* **45**, 1062–1068 (2017).

48. Mardini, S., Alsubaie, S., Cayci, C., Chim, H. & Wetjen, N. Three-dimensional preoperative virtual planning and template use for surgical correction of craniosynostosis. *J. Plast. Reconstr. Aesthetic Surg.* **67**, 336–343 (2014).

49. Seruya, M. *et al.* Computer-Aided Design and Manufacturing in Craniosynostosis Surgery. *J. Craniofac. Surg.* **24**, 1100–1105 (2013).

50. Burge, J. *et al.* Application of CAD/CAM prefabricated age-matched templates in cranio-orbital remodeling in craniosynostosis. *J. Craniofac. Surg.* **22**, 1810–3 (2011).

51. Ni, J., Yang, B. & Li, B. Reconstructive Operation of Nonsyndromic Multiple-Suture Craniosynostosis Based on Precise Virtual Plan and Prefabricated Template. *J. Craniofac. Surg.* **28**, 1541–1542 (2017).

52. Mommaerts, M. Y. *et al.* On the Assets of CAD Planning for Craniosynostosis Surgery. *J. Craniofac. Surg.* **12**, 547–554 (2001).

53. Kobets, A. J. *et al.* Virtual modeling, stereolithography, and intraoperative CT guidance for the optimization of sagittal synostosis reconstruction: a technical note. *Child's Nerv. Syst.* **34**, 965–970 (2018).

54. Frank Baum, L. *The Master Key: An Electrical Fairy Tale, Founded Upon the Mysteries of Electricity and the Optimism of Its Devotees*. (Bobbs-Merrill Company, 1901).

55. Wu, H. K., Lee, S. W. Y., Chang, H. Y. & Liang, J. C. Current status, opportunities and challenges of augmented reality in education. *Comput. Educ.* **62**, 41–49 (2013).

56. Glauser, W. Doctors among early adopters of Google Glass. *Can. Med. Assoc. J.* **185**, 1385 LP – 1385 (2013).

57. Nakhla, J. *et al.* Use of Google Glass to Enhance Surgical Education of Neurosurgery Residents: "Proof-of-Concept" Study. *World Neurosurg.* **98**, 711–714 (2017).

58. Knight, H. M., Gajendragadkar, P. R. & Bokhari, A. Wearable technology: using Google Glass as a teaching tool. *Case Reports* **2015**, bcr2014208768–bcr2014208768 (2015).

59. Iqbal, M. H. *et al.* The effectiveness of Google GLASS as a vital signs monitor in surgery: A simulation study. *Int. J. Surg.* **36**, 293–297 (2016).

60. Drake-Brockman, T. F. E., Datta, A. & Von Ungern-Sternberg, B. S. Patient monitoring with Google Glass: A pilot study of a novel monitoring technology. *Paediatr. Anaesth.* **26**, 539–546 (2016).

61. Yoon, J. W. *et al.* Technical feasibility and safety of an intraoperative head-up display device during spine instrumentation. *Int. J. Med. Robot. Comput. Assist. Surg.* **13**, e1770 (2017).

62. Qian, L. *et al.* Comparison of optical see-through head-mounted displays for surgical interventions with object-anchored 2D-display. *Int. J. Comput. Assist. Radiol. Surg.* **12**, 901–910 (2017).

63. Moosburner, S. *et al.* Real world usability analysis of two augmented reality headsets in visceral surgery. *Artif. Organs* **43**, 694–698 (2019).

64. Pratt, P. *et al.* Through the HoloLens™ looking glass: augmented reality for extremity reconstruction surgery using 3D vascular models with perforating vessels. *Eur. Radiol. Exp.* **2**, 2 (2018).

65. Incekara, F., Smits, M., Dirven, C. & Vincent, A. Clinical Feasibility of a Wearable Mixed-Reality Device in Neurosurgery. *World Neurosurg.* **118**, e422–e427 (2018).

66. Li, Y. *et al.* A wearable mixed-reality holographic computer for guiding external ventricular drain insertion at the bedside. *J. Neurosurg.* **24**, 1–8 (2018).

67. Kuzhagaliyev, T. *et al.* Augmented reality needle ablation guidance tool for irreversible electroporation in the pancreas. in *Medical Imaging 2018: Image-Guided Procedures, Robotic Interventions, and Modeling* (eds. Webster, R. J. & Fei, B.) vol. 10576 30 (SPIE, 2018).

68. Meulstee, J. W. *et al.* Toward Holographic-Guided Surgery. *Surg. Innov.* **26**, 86–94 (2019).

69. Mezger, U., Jendrewski, C. & Bartels, M. Navigation in surgery. *Langenbeck's Arch. Surg.* **398**, 501–514 (2013).

70. Azarmehr, I., Stokbro, K., Bell, R. B. & Thygesen, T. Surgical Navigation: A Systematic Review of Indications, Treatments, and Outcomes in Oral and Maxillofacial Surgery. *J. Oral Maxillofac. Surg.* **75**, 1987–2005 (2017).

71. Kuhlemann, I., Kleemann, M., Jauer, P., Schweikard, A. & Ernst, F. Towards X-ray free endovascular interventions – using HoloLens for on-line holographic visualisation. *Healthc. Technol. Lett.* **4**, 184–187 (2017).

72. Moreta-Martinez, R. *et al.* Augmented reality in computer-assisted interventions based on patient-specific 3D printed reference. *Healthc. Technol. Lett.* **5**, 162–166 (2018).

73. Müller, F. *et al.* Augmented Reality Navigation for Spinal Pedicle Screw Instrumentation using Intraoperative 3D Imaging. *Spine J.* **000**, 1–8 (2019).

74. van Doormaal, T. P. C., van Doormaal, J. A. M. & Mensink, T. Clinical Accuracy of Holographic Navigation Using Point-Based Registration on Augmented-Reality Glasses. *Oper. Neurosurg.* **17**, 588–593 (2019).

75. Frantz, T., Jansen, B., Duerinck, J. & Vandemeulebroucke, J. Augmenting Microsoft's HoloLens with vuforia tracking for neuronavigation. *Healthc. Technol. Lett.* **5**, 221–225 (2018).

76. van Doormaal, T. P. C., van Doormaal, J. A. M. & Mensink, T. Clinical Accuracy of Holographic

Navigation Using Point-Based Registration on Augmented-Reality Glasses. *Oper. Neurosurg.* **0**, 1–6 (2019).

77. Han, W. *et al.* A new method for cranial vault reconstruction: Augmented reality in synostotic plagiocephaly surgery. *J. Cranio-Maxillofacial Surg.* **47**, 1280–1284 (2019).

78. Luijten, G. Holographic augmented reality in deep inferior epigastric perforator flap breast reconstructions. (University of Twente, 2020).

79. Norrdine, A. An Algebraic Solution to the Multilateration Problem An Algebraic Solution to the Multilateration Problem. 11–15 (2015) doi:10.13140/RG.2.1.1681.3602.

80. HoloLens 2 | Microsoft Docs. https://www.microsoft.com/en-us/hololens/hardware (2020). Accesed on 28-01-2020.

81. Eye tracking on HoloLens 2 | Microsoft Docs. https://docs.microsoft.com/en-us/windows/mixed-reality/eye-tracking (2019). Accesed on 28-01-2020.

82. Comfort - Mixed Reality | Microsoft Docs. https://docs.microsoft.com/en-us/windows/mixed-reality/comfort (2019). Accesed on 28-01-2020.

83. Gao, Y., Lin, L., Chai, G. & Xie, L. A feasibility study of a new method to enhance the augmented reality navigation effect in mandibular angle split osteotomy. *J. Cranio-Maxillofacial Surg.* **47**, 1242–1248 (2019).

84. García-Mato, D. *et al.* Craniosynostosis surgery: workflow based on virtual surgical planning, intraoperative navigation and 3D printed patient-specific guides and templates. *Sci. Rep.* **9**, 17691 (2019).

85. Introducing instinctual interactions | Microsoft Docs. https://docs.microsoft.com/en-us/windows/mixed-reality/interaction-fundamentals (2019). Accesed on 28-01-2020.

86. Romanus, T. *et al.* Mid-Air Haptic Bio-Holograms in Mixed Reality Mid-Air Haptic Bio-Holograms in Mixed Reality. (2020).

87. R.F.S & Rushton, M. A. Unilateral Hyperplasia of the Mandibular Condyle. *Proc. R. Soc. Med.* **39**, 431–438 (1946).

88. Broadway, R. T. & Orth, D. Two cases of unilateral hyperplasia of the mandibular condyle. *Proc. R. Soc. Med.* **51**, 691–693 (1958).

89. Ghawsi, S., Aagaard, E. & Thygesen, T. H. High condylectomy for the treatment of mandibular condylar hyperplasia: A systematic review of the literature. *Int. J. Oral Maxillofac. Surg.* **45**, 60–71 (2016).

90. Niño-Sandoval, T. C., Maia, F. P. A. & Vasconcelos, B. C. E. Efficacy of proportional versus high condylectomy in active condylar hyperplasia — A systematic review. *Journal of Cranio-Maxillofacial Surgery* vol. 47 1222–1232 (2019).

91. Fariña, R. *et al.* High condylectomy versus proportional condylectomy: Is secondary orthognathic surgery necessary? *Int. J. Oral Maxillofac. Surg.* **45**, 72–77 (2016).

92. Kubben, P. & Sinlae, R. Feasibility of using a low-cost head-mounted augmented reality device in the operating room. *Surg. Neurol. Int.* **10**, (2019).

93. Buchanan, E., Xue, Y., Xue, A., Olshinka, A. & Lam, S. Multidisciplinary care of craniosynostosis. *J. Multidiscip. Healthc.* **10**, 263–270 (2017).